PEOPULE'S DEMOCRATIC REPUBLIC OF ALGERIA

Higher Education and Scientific Research Ministry

University of Echahid Hamma Lakhdar

El- Oued

N° ordre :

N° series:

Faculty of Exact Sciences

Department of Physics

MEMORY

Presented to obtain the master's diploma in applied physics :

Radiation and Energy

by :

Nemsi Fatma

Djedidi Ouarda

Title

Dosimetric characteristics of RPL GD-302 and RPL GD-450: Percentage Dose Depth and Energy response for electrons beams.

Sustained : 08 / 06 / 2017

Before the jury composed of :

President :	BEGGAS Azzeddine	MAA	University El-Oued
Examiner :	LITIM Fethi	MAA	University El-Oued
Examiner :	BEGI Mohamed	MAA	University El-Oued
Trainer:	BENALI Abdelhai	MAA	University El- Oued

University season: 2016/2017

I dedicate this work to

My best people for me

My parents

My brothers and my sister

All my family

Nemsi Fatma

I dedicate this modest work

To my best people

My dear parents

My brothers and my sisters

All my family

DJEDIDI OUARDA

ACKNOWLEDGEMENTS

In the Name of Allah, the Most Merciful, the Most Compassionate all praise is to Allah, the Lord of the worlds; and prayers and peace be upon Mohamed His servant and messenger.

First and foremost, we must acknowledge our limitless thanks to Allah, the Ever-Magnificent; the Ever-Thankful, for His help and bless.

We owe a deep debt of gratitude to our trainer ***M. Benali Abdelhai,*** *a who worked hard with us from the beginning till the completion of the present research.*

We would like to express deepest gratitude for each ***M. Beggas Azzeddine****, and* ***M. Begi Mohamed*** *, also* ***M. Litim Fethi*** *to accept them to discuss our memory.*

We cannot express enough thanks to ***M. Becer Zoubir*** *on his advices, and our university for giving us an opportunity to complete this work.*

Last but not least, we would like to express our wholehearted thanks to our family for their generous support.

REFERENCES

TABLE OF CONTENTS

CHAPTER III : MONTE CARLO SIMULATION

CHAPTERIV : OPTIMIZING OF REPENSE ENERGYAND PERSENTAGE DOSE DEPTH

Liste of figures

Liste of tables

Nomenclature

Lettres latin & Symbols Greek

E_B	the binding energy of the electron
m_c	Kinetic mass electron
Z	Atomic number
h	Planck constante [J.s]
z	charge of the particle divided by the proton charge
dN	Number of electrons.
dx	Thickness of absorbent matter
D	Absorbed dose
Gy	unit for absorbed dose
H_T	Equivalent dose
E	Effective dose
W_R	Weighting factor
W_T	Weighting factor tissue
$D_{T,R}$	Average dose absorbed in an argon or tissue
σ	cross section
μ	Coefficient of proportionality
q	particle charge
ρ	density of the material
a	radius of atom

Acronyms

IAEA	International atomic energy agency
ICRP	International commission on radiological protection.
ICRU	International commission on radiation units and measurements
TLD	Thermoluminescence dosimeter
OSL	Optically stimulated luminescent dosimeter
RPL	Radiophotoluminescence glass dosimeter
PENELOPE	Pe netration and energy loss of positons and electrons
GEANT4	G eometry and tracking
MCNP	Monte carlo N-particle
LANL	Los alamos national laboratory
PMMA	polymethylmethacrylate
MC	Monte Carlo
SSD	Source-to-Surface Distance

Nomenclature

R_{50}	Depth where the dose falls to 50% of the maximum dose
PDD	Percent Depth Dose

INTRODUCTION

INTRODUCTION

Since the beginning of humanity, radiation is located in the universe, and after about 100 years which since the discovery of X- ray by the scientist Rontgen (1895) then the scientist Becquerel and his discovery of radioactivity (1896), in rolled discoveries in this domain even has become a life more sophisticated in recent decades, it has swept the ionizing radiation a private many sectors of which agricultural and military, as well as the medical world became so called medicine radiation [1].

In any application or domain type, it must find out of measurement physical quantities represented in the absorbed dose which is measured by gray and individual monitoring through the interaction of radiation with matter. In generally, to determine these dosimeters quantities passive or active, we define the main physical quantities.

In this memory, we will examine the dosimeter passive called Radiophotoluminescence glass dosimeter (RPLGD), this dosimeter is a glass phosphate –doped silver. It emits fluorescence orange by excitation UV when the glass was previously exposed to ionizing radiation. The intensity of this fluorescence is proportional to the dose. This technique then offers all a set of benefits for monitoring routine, which includes a holding fast data, reuse detectors, insentivity in the light, to the temperature and humidity, and stability of signal. Where by reader system we can find out of intensity and absorbed dose of detector [2-5]. The method will be adopted in this thesis is simulation program called Monte Carlo, will be used this simulation to estimate the value of the energy dependence, and the percentage depth-dose (PDD) of two dosimeters Radiophotoluminescence, commercially known as RPL GD- 450 and RPL GD- 302.

This current work has four chapters, first chapter will be allocated the most important interaction of radiation for photons and electrons, in chapter two we will discuss the physical quantities and detectors with mention of characteristics and also uses of this detectors which will be remembered Thermoluminescence dosimeter (TLD), Optically stimulated luminescent dosimeters (OSLD), and in particular Radiophotoluminescence glass dosimeter (RPLGD). The third chapter we will discuss the method used in this study, which is simulation program with Monte Carlo method, we have cited a general description of this method and the main code implemented in this work namely code MCNP (Monte Carlo N-Particles) which is developed by the national laboratory of Los Alamos(LANL). For last chapter, which is our experimental work, a simulation Monte Carlo (MC) code MCNP version 5,we will be used to optimize the energy

dependence of radiophotoluminescence dosimeters RPL GD- 450 and RPL GD- 302and the percentage depth dose (PDD), after a citation of the materials and methods that are used in this study, and finished with the results that are obtained with their discussion.

Finally we conclude this memory with a general conclusion, discuss about the dependence energy of both dosimeters radiophotoluminescence (GD- 450 and GD- 302) and the calculated percentage depth dose (PDD).

CHAPTER I
INTERACTION RADIATION – MATTER

CHAPTER I
INTERACTION RADIATION – MATTER

In this chapter, we summarize what happens and the main laws that govern the interaction of radiation with matter.

I.1.Radiation

The term radiation applies to the emission and propagation of energy through space or a material medium [6], this energy it becomes the form of waves or streams of particles [7].

I.1.1.Classification of radiation

Radiation is classified into two main categories, non ionizing and ionizing, depending on its ability to ionize matter.

● Non-ionizing radiation (cannot ionize matter).

● Ionizing radiation (can ionize matter either directly or indirectly) :

— Directly ionizing radiation (charged particles) : electrons, protons, a particles and heavy ions.

— Indirectly ionizing radiation (neutral particles) : photons (X-rays and gamma rays), neutrons [1, 8, 9].

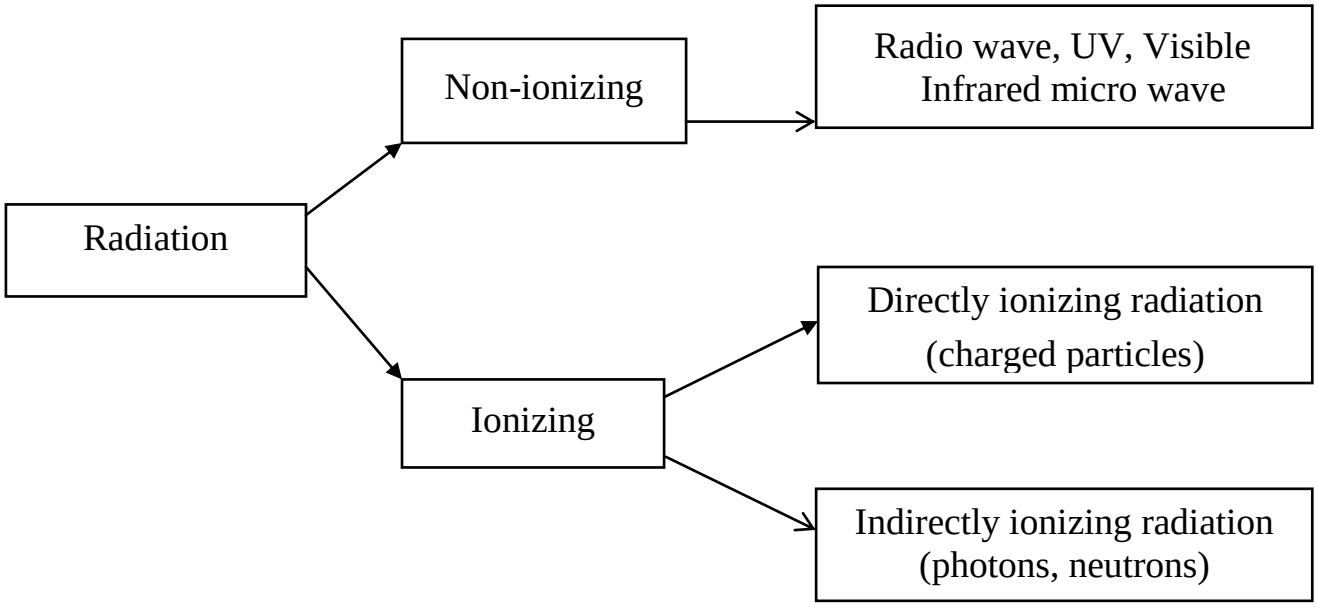

Figure (I.1) : Classifications of radiation [1, 9].

I.2.Interaction photons with matter

Photons are electromagnetic radiation [10] have the ability in penetration of matter. The energy of photon : $E = h\upsilon$, photons react with matter by three basic processes : Photoelectric effect, Compton effect, Pair production.

I.2.1.Photoelectric effect

In the photoelectric effect the photon interacts with a tightly bound orbital electron of an attenuator and disappears, while the orbital electron is ejected from the atom as a photoelectron with a kinetic energy E_e given by [11] :

$$Ee = E_0 - E_B \tag{I.1}$$

where E_0 is the incident photon energy ($E_0 = h\upsilon$) and E_B is the binding energy of the electron in its original shell [1,11].

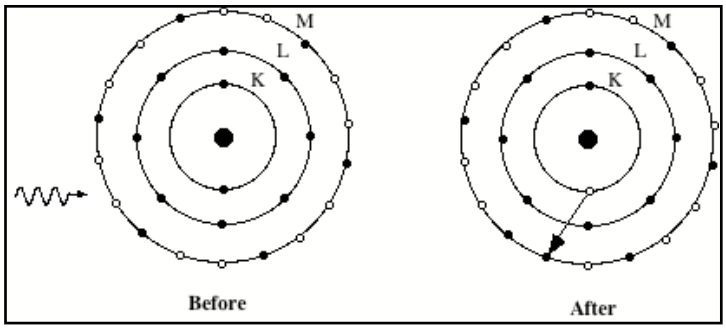

Figure (I.2) : photoelectric effect.

Discontinuities in photoelectric cross section due to discrete binding energies of atomic electrons and it is formula [11] :

$$\sigma_P = \frac{32}{3}\sqrt{2}\,\pi r_e^2 \alpha^4 Z^5 \left(\frac{m_e c^2}{E_0}\right)^{7/2} \tag{I.2}$$

Exact cross section calculations are difficult due to atomic effects : the photon electric cross-section scales with Z^5, this means that high-Z detectors are more efficient at high energies.

I.2.2.Compton effect

In the Compton effect, the photon scatters from a free electron or a loosely bound atomic electron. The scattered photon has less energy than the incident photon and the excess energy is

transferred to the electron. The laws of conservation of mass-energy and conservation of momentum limit the maximum kinetic energy of the photoelectron to a value [6, 11, 12] :

$$E_f = \frac{E_0}{[1+\gamma(1-\cos\theta)]} \qquad \textbf{(I.3)}$$

$\gamma = \frac{E_0}{m_0 c^2}$ and $\cos\theta = -(1+\gamma)\tan(\frac{\phi}{2})$ and $E_f = h\upsilon'$

And the information that clarified the relationship (I.3) is that the greater the scatter angle θ decreased energy E_f [1, 11, 13, 14].

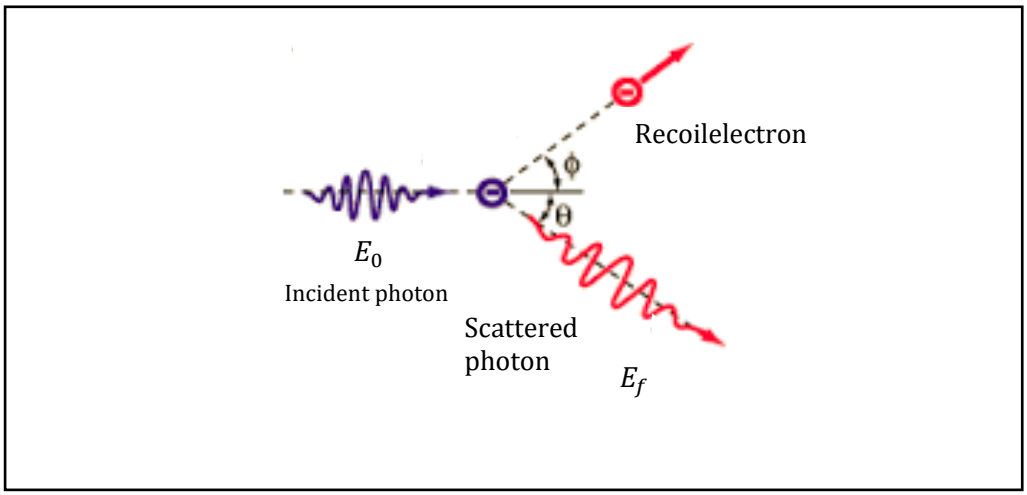

Figure (I.3) : Compton effect.

The differential cross-section per unit of solid angle of the Compton effect is given by the formula of Klein-Nishina [5, 15] :

$$\frac{d\sigma_c}{d_\Omega} = r_0^2 \frac{1+\cos^2\theta}{2} \frac{1}{[1+\alpha(1-\cos\theta)]^2} \left\{1 + \frac{\alpha^2(1-\cos\theta)^2}{(1+\cos^2\theta)[1+\alpha(1-\cos\theta)]}\right\} \qquad \text{(I.4)}$$

Where: $\alpha = {}^{E_0}/_{m_e c^2}$

I.2.3.Pair production

In pair production a high energy photon is transformed into an electron-positron pair :

$$\gamma \longrightarrow e^+ + e^-$$

This process cannot happen in free space it needs the presence of a third body, usually a nucleus, to simultaneously conserve energy and momentum. Since the rest energy of an electron is 0.51 MeV, pair production is energetically impossible for photon energies less than 1.02 MeV.

However when pair production becomes possible it soon becomes the dominant interaction process for beams of very high energy photons [12, 14, 15].

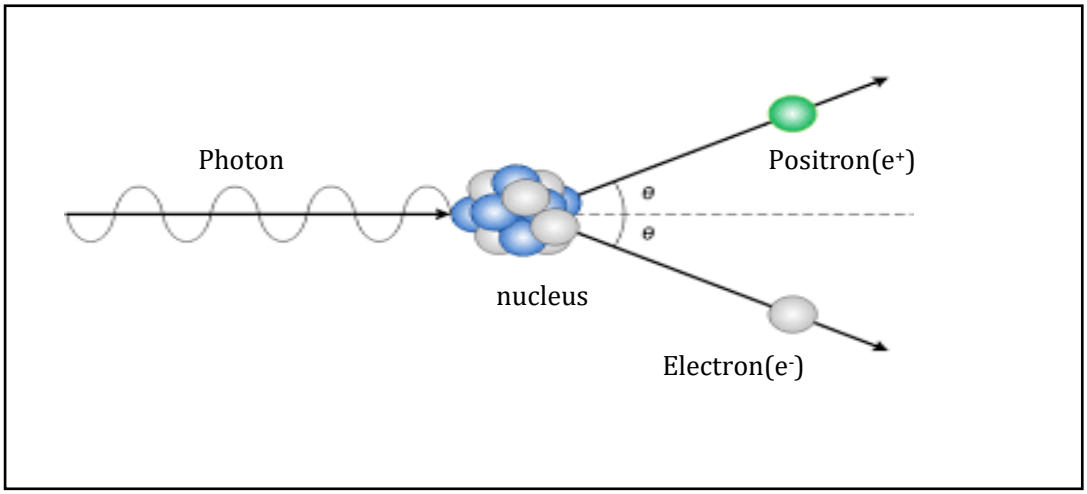

Figure (I.4) : Pair production.

The cross section σ_n for pair production in the field of a nucleus varies as [15] :

$$\sigma_n \sim Z^2 \tag{I.5}$$

Cross sections for the most probable individual processes by which photons interact with atoms and is derived as :

$$\sigma_{tot} = \sigma_p + \sigma_c + \sigma_n \tag{I.6}$$

I.3.Interactions of light charged particles

Whereas photons interact with matter by photoelectric, Compton, or pair production process, charged particles (electrons, protons, γ particles, and nuclei) interact principally by ionization and excitation. Radiative collisions in which the charged particle interacts by the bremsstrahlung process are possible but are much more likely for electrons than for heavier charged particles.

The charged particle interactions or collisions are mediated by Coulomb force between the electric field of the traveling particle and electric fields of orbital electrons and nuclei of atoms of the matter. Collisions between the particle and the atomic electrons result in ionization and excitation of the atoms. Collisions between the particle and the nucleus result in radiative loss of energy or bremsstrahlung. Particles also suffer scattering without significant loss of energy.

Because of much smaller mass, electrons suffer greater multiple scattering than do heavier particles.

I.3.1.Stopping power

The rate of kinetic energy loss per unit path length of the particle (-dE/dx) is known as the stopping power (S), used to describe the gradual loss of energy of the charged particle as it penetrates into an absorbing medium. Two classes of stopping powers are known :

collision (ionization and excitations) stopping power that results from charged particle interaction with orbital electrons of the absorber and radiative stopping power that results from charged particle interaction with nuclei of the absorber (bremsstrahlung production).

The quantity S/ρ is called the mass stopping power, where ρ is the density of the medium and is usually expressed in MeV cm^2/g [6, 9].

I.3.1.1.The Linear Energy Transfer (LET)

When discussing the biological effects of radiation the term 'Linear Energy Transfer' (LET) is often used to refer to the energy loss of charged particles. The linear energy transfer is defined as the amount of energy transferred, per unit track length, to the immediate vicinity of the trajectory of the charged particle. For heavy and low-velocity particles, the energy loss per unit track length and the LET are the same. For light and fast particles, however, the two quantities differ considerably. Part of the energy loss of an electron of several MeV is used to eject energetic δ-electrons from the atoms in the medium. These energetic electrons do not deposit their energy in the immediate vicinity of the track and therefore do not contribute to the LET.

The energy loss of a high-energy charged particle in matter due to its interactions with the electrons present in the matter is given by the Bethe-Bloch equation approximated :

$$\frac{dE}{dx} \approx \rho(2MeV\ cm^2/g)\frac{z^2}{\beta^2} \qquad (I.7)$$

Where :

$\frac{dE}{dx}$: energy loss of particle per unit length ;

z : charge of the particle divided by the proton charge ;

β : relativistic parameters ;

ρ : density of the material ;

So the Linear Energy Transfer (LET) is similar to the stopping power except that it does not include the effects of radiative energy loss (i.e., Bremsstrahlung) or delta-rays [14].

I.4.Interaction electrons with matter

Electron is a stable elementary particle with a negative electric charge of $1.6x10^{-19}$ coulombs and a mass of 9.1×10^{-31} kg [7]. As an energetic electron traverses matter, it interacts with matter through Coulomb interactions with atomic orbital electrons and atomic nuclei. Through these collisions the electrons may lose their kinetic energy (collision and radiative losses) or change their direction of travel (scattering). Energy losses are described by stopping power, and scattering is described by scattering power.

The collisions between the incident electron and an orbital electron or nucleus of an atom may be elastic or inelastic. In an elastic collision the electron is deflected from its original path but no energy loss occurs, while in an inelastic collision the electron is deflected from its original path and some of its energy is transferred to an orbital electron or emitted in the form of :

- Bremsstrahlung (X ray)
- Secondary electron (the ejected electron, of low energy, is called secondary electron SE)
- Auger electrons (ejected electrons with an energy characteristic from the target atoms).

Energetic electrons experience thousands of collisions as they traverse an absorber ; hence their behavior is described by a statistical theory of multiple scattering embracing the individual elastic and inelastic collisions with orbital electrons and nuclei [1, 16].

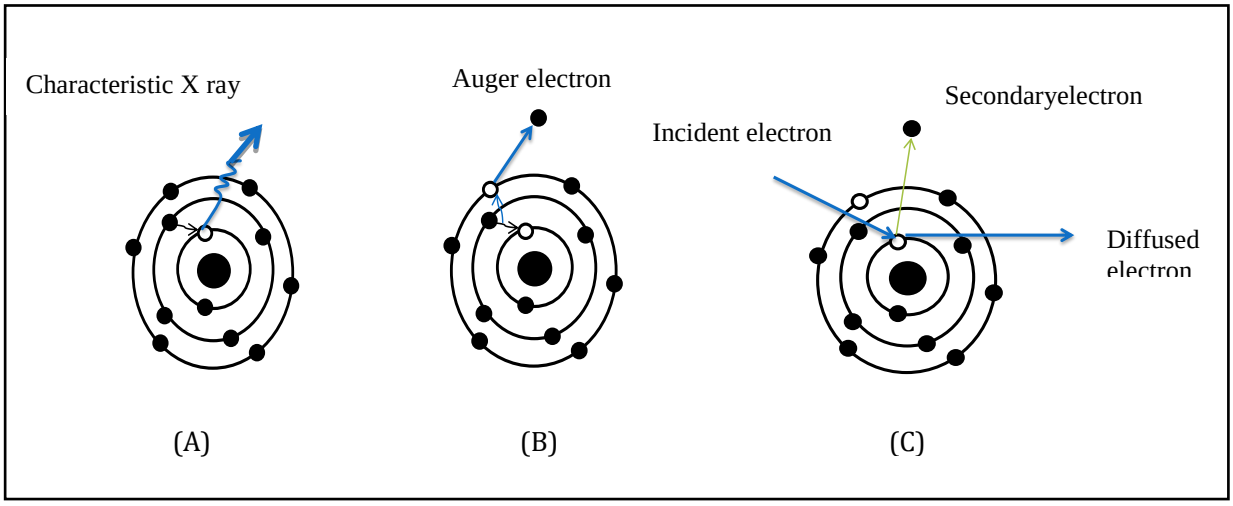

Figure (I.5) : Interaction of an electron with electrons orbital : (A) Bremsstrahlung, (B) Secondary electron and (C) Auger electrons [17].

I.4.1.Electron–orbital electron interactions

Coulomb interactions between the incident electron and orbital electrons of an absorber result in ionizations and excitations of absorber atoms :

- Ionization : ejection of an orbital electron from the absorber atom.
- Excitation : transfer of an orbital electron of the absorber atom from an allowed orbit to a higher allowed orbit (shell).

Atomic excitations and ionizations result in collisional energy losses and are characterized by collision (ionization) stopping powers(-dE /dx) :

$$S_{Col} = \left(-\frac{dE}{dx}\right)_{Col} \tag{I.8}$$

The signal (-) means the greater distance incursion in matter increased loss electrons energy. The range R of a charged particle in a particular absorbing medium is an experimental concept providing the thickness of an absorber that the particle can just penetrate. It depends on the particle's kinetic energy, mass as well as charge, and on the composition of the absorbing medium. Various definitions of range that depend upon the method employed in the range determinations are in common use.

I.4.1.1.The range of charged particles(electrons)

Generally, the concepts of range R must be distinguished from the concept of the path-length of a charged particle. This path-length simply provides the total path-length of the charged particle in the absorber and can be calculated, using the continuous slowing down approximation (CSDA) as follows :

$$\overline{R}_{CSDA} = \int_0^R dx = \int_0^\infty \frac{dx}{dE} dE = \int_0^{E_0} \left(-\frac{dE_x}{dx}\right)^{-1} dt \tag{I.9}$$

For light charged particles (like electrons) $\overline{R}_{CSDA}$ is up to twice the range of charged particles in the absorber, because of the very tortuous path that the lightcharged particles experience in the absorbing medium, but for heavy charged particles (photons) do not experience radiative losses, transfer only small amounts of energy in individual ionizing collisions with orbital electrons, and mainly suffer small angle deflections in elastic collisions. Their path through an absorbing medium is thus essentially rectilinear, as shown schematically in Figure (I.6) :

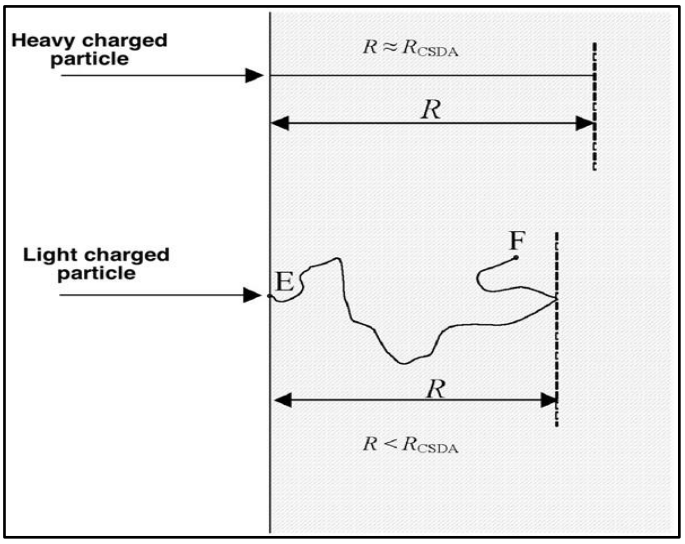

Figure (I.6) : Schematic diagram of charged particle penetration into a medium. Top:Heavy charged particle; bottom: light charged particle (electron) [9].

So, the maximum range given to the following relationship with enough energy of ionization :

$$R_{max}\left[\frac{g}{cm^2}\right] = \begin{cases} 0.412E_0^{1.265-0.0955\ln(E_0)} & 0.0111MeV \leq E_0 \leq 2.5MeV \\ 0.530E_0^{-0.106} & E_0 > 2.5MeV \end{cases} \quad (I.10)$$

Where E_0 is Electron kinetic energy (MeV) [1, 18].

I.4.2.Electron–nucleus interactions

Because of its small mass, an electron may interact with the electromagnetic field of a nucleus and be decelerated so rapidly that a part of its energy is lost as bremsstrahlung. The rate of energy loss as a result of bremsstrahlung increases with the increase in the energy of the electron and the atomic number of the medium. Bremsstrahlung production is governed by the Larmor relationship, which states that the power 'P' emitted in the form of photons from an accelerated charged particle is proportional to the square of the particle acceleration 'a' and the square of the particle charge 'q' [1] :

$$P = \frac{q^2a^2}{6\pi\varepsilon_0 c^3} \quad (I.11)$$

In this type of interactions, when the electron undergoes with a particular atom of radius a depends on the impact parameter 'b' of the interaction, defined as the perpendicular distance between the electron direction before the interaction and the atomic nucleus (see Fig.I.7).

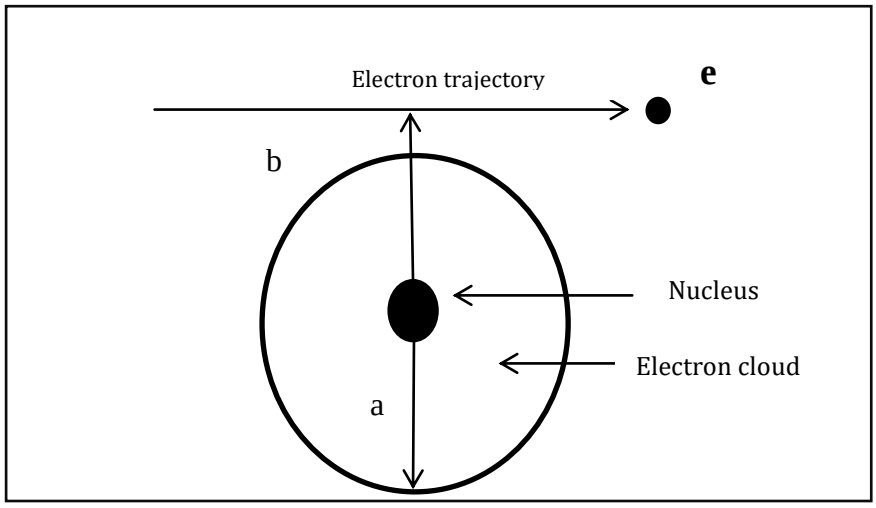

Figure (I.7) : Interaction of an electron with an atom, where a is the atomic radius and b is the impact parameter [1].

- For b >> a the electron will undergo a soft collision with the whole atom and only a small amount of energy will be transferred from the incident electron to orbital electrons.
- For b = a the electron will undergo a hard collision with an orbital electron and an appreciable fraction of the electron's kinetic energy will be transferred to the orbital electron.
- For b << a the incident electron undergoes a radiative interaction (collision) with the atomic nucleus. The electron will emit a photon (bremsstrahlung) with energy between zero and the incident electron kinetic energy. The energy of the emitted bremsstrahlung photon depends on the magnitude of the impact parameter b ; the smaller the impact parameter, the higher the energy of the bremsstrahlung photon. The relationship of stopping power (radiative stopping power) of this case :

$$S_{Rad} = \left(-\frac{dE}{dx}\right)_{Rad} \qquad (I.12)$$

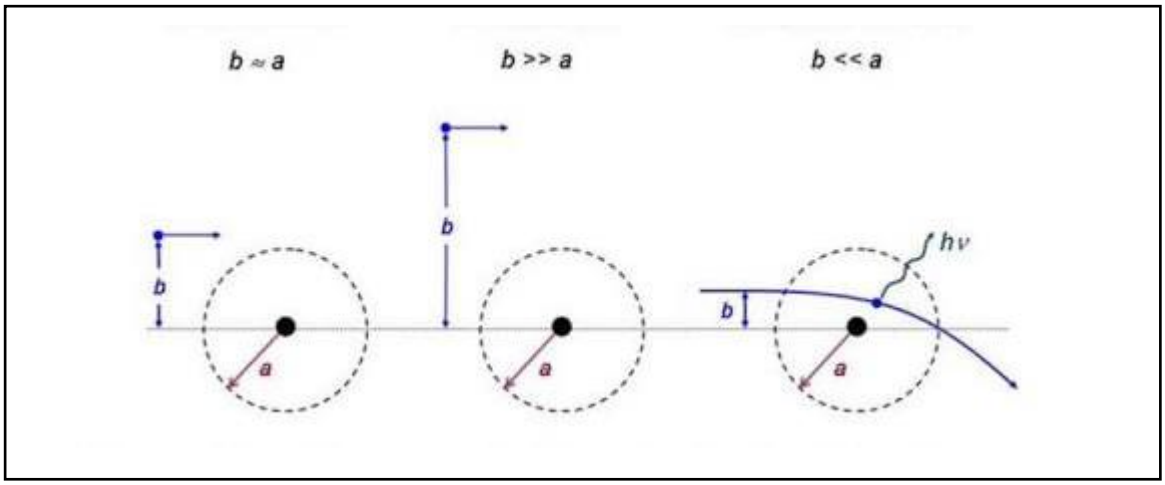

Figure (I.8) : Three different types of collisions of a charged particle with an atom: Hard collision, soft collision, and radiative collision [9].

As we made clear already, the inelastic energy losses by an electron moving through a medium with density ρ are described by the total mass–energy stopping power $(S/\rho)_{tot}$, $(S/\rho)_{tot}$ consists of two components : the mass collision stopping power $(S/\rho)_{col}$, and the mass radiative stopping power$(S/\rho)_{rad}$ [1, 9] :

$$\left(-\frac{dE}{dx}\right)_{tot} = \left(-\frac{dE}{dx}\right)_{Col} + \left(-\frac{dE}{dx}\right)_{Rad} \tag{I.13}$$

$$\left(\frac{1}{\rho}\frac{dE}{dx}\right)_{tot} = (S/\rho)_{tot} \tag{I.14}$$

So :

$$(S/\rho)_{tot} = (S/\rho)_{Col} + (S/\rho)_{Rad} \tag{I.15}$$

The bremsstrahlung cross section σ_b , which gives the radiation emission probability, depends on the strength of the nuclear Coulomb force, which in turn depends on the atomic number and how close the encounter is. The bremsstrahlung cross section varies as :

$$\sigma_b \sim Z^2 r_e^2 f(E) = Z^2 \left(\frac{e^2}{m_e c^2}\right)^2 f(E) \tag{I.16}$$

Where

Z is the nucleus atomic number, $r_e \equiv \frac{e^2}{m_e c^2}$ is the classical electron, and radius = 2.82×10^{-13} cm. The function f(E) is a strongly increasing function of initial energy E that becomes appreciable

only for E > $m_e c^2$, the electron rest mass energy. The resulting average energy loss per length traversed in a medium due to the emission of bremsstrahlung radiation varies as :

$$\left(-\frac{dE}{dx}\right)_{Rad} \sim NE\sigma_b \quad (I.17)$$

Where E is the incoming beta energy, N is the number density of atoms [11].

I.4.3.Cherenkov radiation

While playing an important role in the detection of very high energy charged particles, absorbs only a small amount of energy. The contribution of each mechanism depends on the charge, mass and speed of the incident particle as well as the atomic numbers of the elements which make up the absorbing material. Cherenkov radiation is When the particle moves faster than the speed of light in the material it generates a shock wave of electromagnetic radiation similar to the bow wave produced by a boat travelling faster than the speed of water waves. Cherenkov radiation does not occur at all if the particle's speed is less than the speed of light in the material. Even at high energies the energy lost by Cherenkov radiation is much less than that by the other two mechanisms but it is used in radiation detectors where the ionization along the track cannot be conveniently measured [12].

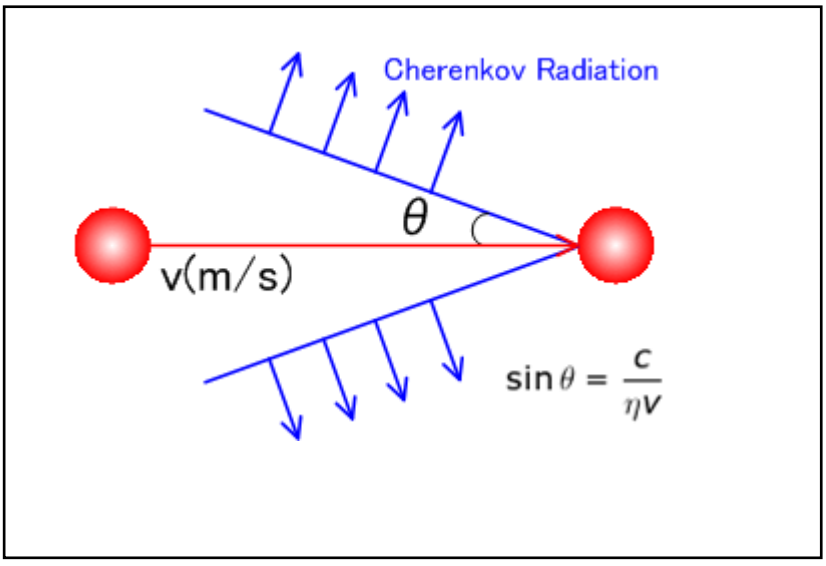

Figure (I.9) : Cherenkov radiation

I.4.4.Absorption of electrons

The behavior of electrons when the fall to matter (charged particle) is different from a significant difference for the behavior of heavy particle, some of different in the impact of the electron in matter, not be this impact in the form straight line, but in the form of line refracted, a

charged particle penetrates in matter. It loses energy by transferring a small amount of energy to each of a large number of electrons along its trajectory. Some of these electrons have enough energy to travel a macroscopic distance, and also cause further ionization along their trajectory in addition to that the completely different for a range, so electrons do not have a well-defined range, shape shows that :

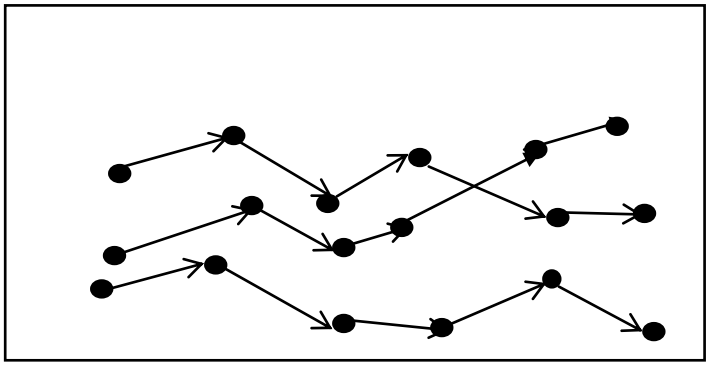

Figure (I.10) : the impact of the electron in matter.

That the fall of the beam parallel of electrons with energy one on the matter so called absorbent matter, if the thickness of this matter is not enough to absorb this electron, these recent graduated from the other side with matter different cards significant difference (dispersion). Output the feat that the very large compared with his counterpart in the case of heavy particles [2, 4, 13] so because of its light mass an electron is easily scattered in collisions with other electrons. The resulting erratic path will be longer than the linear penetration (range) into the material and there will be greater straggling [12].

I.4.5. Attenuation low

When the scattering electrons is happening, the absorption of these electrons (particles) within the matter, absorption relationship writes as follows :

$$dN = -\mu N_0 dx \qquad \Rightarrow \qquad N = N_0 e^{-\mu x} \tag{I.18}$$

Where:

N : Number of electrons.

N_0: Number of electrons fallen.

x : Thickness of absorbent matter.

μ : Coefficient of proportionality.

This relationship is valid even when the interaction of photon with matter.

The signal (-) means the whenever decrease number of photon or electrons which penetrate the matter increased distance of penetration in this matter.

Traditionally it instead of the expense of the number of electrons or photon use the intensity of radiation' I' :

$$dI = -\mu I_0 dx \tag{I.19}$$

The integration of the relationship (I.19), we find :

$$I = I_0 e^{-\mu x} \tag{I.20}$$

$$\Longrightarrow I_T = \sum_i I_{0i} e^{-\mu_i(E)x} \tag{I.21}$$

I_0: Intensity of radiation which penetrate the matter.

I_T : Intensity of radiation fallen to the matter.

The relationship (I.18) called "law of attenuation" [1, 18].

CHAPTER II

DOSIMETRIC QUANTITIES AND DOSIMETERS

CHAPTER II

DOSIMETRIC QUANTITIES AND DOSIMETERS

The radiation dosimetric systems have been developed for more than 50 years and are applied in the measurement of clinical and environment radiation dose. It deals with methods for a quantitative determination of energy deposited in a given medium by directly or indirectly ionizing radiations.

In this chapter, we have defined the main physical and dosimetric, units used in dosimetry, processes that depend upon these devices and the three kinds of luminescent dosimeters.

II.1. Quantities used in radiation protection and dosimetry

II.1.1. Physical and dosimetric quantities

II.1.1.1. Particle Flow

The particle flow can be defined as being the quotient dN by dt, where dN is the number of particles incident, for a time interval dt[1]:

$$\dot{N} = \frac{dN}{dt} \tag{II.1}$$

II. 1.1.2. Energy flow

Energy flow is defined as the quotient dEby dt, where is the energy particles incident, dt the time interval expressed (W or $j.s^{-1}$) [1]:

$$\dot{E} = \frac{dE}{dt} \tag{II.2}$$

II. 1.1.3. Particulate fluenceand particulatefluence rate

The particle fluence$\emptyset$ is the quotient dNby da, where dNis the number of particles incident on a sphere of cross-sectional area da:

$$\emptyset = \frac{dN}{da} \tag{II.3}$$

The unit of particle fluence is m^{-2}.

The particle fluence rate ∅is the quotient of d∅ by dt, where d∅ is theincrement of the fluence in time interval dt:

$$\dot{\emptyset} = \frac{d\emptyset}{dt} \tag{II.4}$$

with units of $m^{-2}.s^{-1}$[1].

II. 1.1.4. Energy fluenceand energy fluence rate

The energy fluence is the quotient of dE by da, where dE is the radiant energy incident on a sphere of cross-sectional area da :

$$\Psi = \frac{dE}{da} \tag{II.5}$$

The unit of energy fluence is J/m^2. Energy fluence can be calculated from particle fluence by using the following relation:

$$\Psi = \frac{dN}{da} \times E = \emptyset \times E \tag{II.6}$$

where E is the energy of the particle and dN represents the number of particles with energy E.
The energy fluence rate (also referred to as intensity) is the quotient ofd Ψby dt, where dΨis the increment of the energy fluence in the time interval dt:

$$\dot{\Psi} = \frac{d\Psi}{dt} \tag{II.7}$$

The unit of energy fluence rate is W/m^2 or $J.m^{-2}.s^{-1}$[1].

II. 1.1.5. Energy imparted

the energy imparted of the matter in the volume is defined as :

$$\epsilon_i = R_{in} - R_{out} + \Sigma Q \tag{II.8}$$

R_{in} is the radiant energy that enters the volume.
R_{out} is the energy that leaves.
ΣQ is the sum of all changes in the mass energy of the nuclei and particles which result from all the transformations that occur in the volume [19].

II. 1.1.6. Energy deposited

The energy deposited in a given volume is defined as the sum of all energy imparted in this volume [19, 20]:

$$\epsilon = \sum \epsilon_i \tag{II.9}$$

II. 1.1.7. Absorbed dose and absorbed dose rate

The non-stochastic quantity absorbed dose is defined as the statistical average of the energy imparted per unit mass at a point In spit D is a point quantity, it should be recognized that the physical process does not allow dm to approach zero in the mathematical sense[21].
The absorbed dose is defined as:

$$D = \frac{d\epsilon}{dm} \tag{II.10}$$

where $d\epsilon$ is the mean energy imparted to matter of mass dm by ionising radiation.
The SI unit for absorbed dose is joule per kilogram (J. kg^{-1}) and its special name is gray (Gy) [21,22].
The rate of absorbed dose $\dot{D}$ is the quotient dD by dt where dD is the increment of the dose absorbed and dt the time interval.

$$\dot{D} = \frac{dD}{dt} \tag{II.11}$$

Its unit is joule per kilogram per second ($J.kg^{-1}.s^{-1}$) or gray per second ($Gy.s^{-1}$).

II. 1.1.8. KERMA and KERMA rate

The KERMA (Kinetic Energy Release per unit MAss)its transfer of radiant energy from uncharged primaryto charged particles as they interact in a material.
Energy transferred can be absorbed locally or at a distance[17]:

$$K = \frac{dE_{tr}}{dm} \tag{II.12}$$

the unit OF KERMA is the gray (Gy) : 1Gy = 1 $j.kg^{-1}$.
The flow of KERMA is the quotient dK by dt; Where dK is the increment of KERMA, dt the time interval:

$$\dot{K}=\frac{dK}{dt} \quad \text{(II.13)}$$

Its unit is joule per kilogram per second ($J.kg^{-1}.s^{-1}$) or gray per second ($Gy.s^{-1}$).

II.1.2. Protection Quantities

Dose quantities that the Commission has developed for radiological protection that allow quantification of the extent of exposure of the human body to ionizing radiation from both whole and partial body external irradiation and from intakes of radio nuclides [22].

The protection quantities are equivalent dose in tissues or organs, and effective dose [17].

II. 1.2.1.Equivalent dose

The equivalent dose is the dose absorbed by tissue T or organ. [3, 7] The dose equivalent in tissue or organ is defined as:

$$H_T = \Sigma D_{T,R} \times W_R \quad \text{(II.14)}$$

Where $D_{T,R}$ is the mean absorbed dose in an organ or tissue T of the absorbed dose of the radiation R;

W_R is a radiological weighting factor that takes into account the nature of the radiation.

The unit of equivalent dose is $J.Kg^{-1}$, it is called the Sievert (Sv)[21]. According to the recommendations of the ICRP 103, the weighting factors are summarized in the Table (II.1).

Table (II.1) : Radiation weighting factors[6, 23].

Radiation	w_R
Photons, electrons and muons of all energies	1
Neutrons	See Fig.(II-1)
Protons	2
Alpha particles and heavy ions	20

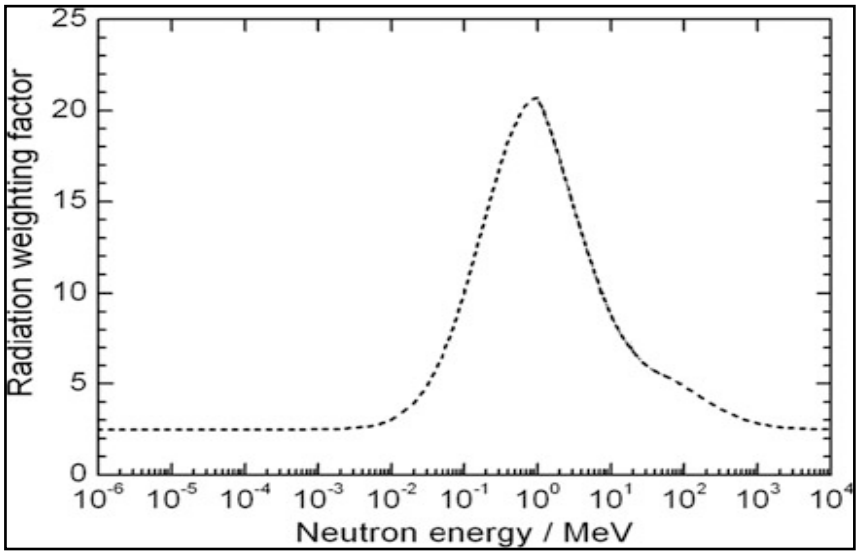

Figure(II.1): Radiation weighting factors$w_R$for external neutron exposure for neutrons of various, energies [23].

II. 1.2.2.Absorbed dose

The amount of energy absorbed by irradiated matter per unit mass. This reflects theamount of energy deposited by ionizing radiation as it passes through a medium (such as air, water orliving tissue) The unit ofabsorbed dose is(Gy)[7].

II. 1.2.3. Effective dose

The effective dose is the sum of the weighted equivalent doses, delivered to the various organs and tissues of the body by internal and external irradiation; she is defined by the formula [6, 7]:

$$E = \Sigma W_T \times H_T = \Sigma W_T \times \Sigma W_R D_{T,R} \quad \text{(II.15)}$$

The unit of effective dose is the Sievert (Sv)[6, 21]**.**

Table (II.2) : Organ/tissue weighting factors [6].

Organ/tissue	w_T	ΣW_T
Bone marrow, colon, lung, stomach, breast, remainder.	0.12	0.72
Gonads.	0.08	0.08
Bladder, liver, oesophagus, thyroid.	0.04	0.16
Bone surface, skin, brain, salivary glands.	0.01	0.04

II.1.3.Individual monitoring

Individual monitoring is the measurement of radiation doses received by individuals working with radiation. Individuals who regularly work in controlled areas or those who work full time in supervised areas should wear personal dosimeters to have their doses monitored on a regular basis. Individual monitoring is also used to verify the effectiveness of radiation control practices in the workplace. It is useful for detecting changes in radiation levels in the workplace and to provide information in case of accidental exposures[3].

II. 1.3.1.Operational Quantities

The human body-related protection quantities, equivalent dose in an organ/tissue and effective dose, are not measurable. To overcome these practical difficulties for external photon irradiation, ICRU [15,24] has introduced and defined a set of operational quantities, which can be measured and which are intended to provide are a son able estimate for the protection quantities. These quantities aim to provide a conservative estimate for the value of the protection quantity avoiding both underestimation and too much overestimation. The operational quantities are based on point doses determined at defined locations in defined phantoms.

II. 1.3.1.1.Operating magnets for the ambient dosimeter

One such phantom is the ICRU-sphere It is a sphere of 30 cm diameter with a density of 1 g/cm^3 and a mass composition of 76.2% oxygen, 11.1% carbon, 10.1%hydrogen and 2.6% nitrogen[22].

II. 1.3.1.2.Ambient Dose Equivalent

The ambient dose equivalent, H*(10), is the operational quantity for area monitoring. It is the dose equivalent at a point in a radiation field that would be produced by the corresponding expanded and aligned field in a 30cmdiameter sphere of unit density issue (ICRU-sphere) at a depth of 10 mm on the radius vector opposing the direction of the aligned field. An oriented and expanded radiation field is an idealized radiation field which is expanded and in which the radiation is additionally oriented in one direction. How radiation protection instruments are calibrated in this quantity is described below [21].

II. 1.3.1.3.The Directional Dose Equivalent

The directional dose equivalent H′ (d,Ω) at the point of interest in the actual radiation field is the dose equivalent which would be generated in the associated expanded radiation field at a depth

of d mm on the radius of the ICRU-sphere which is oriented in the fixed direction 0.03 the depth 0.07 mm and we can write H′(0.07,Ω) [5].

II. 1.3.1.4.Personal Dose Equivalent

The personal dose equivalent, Hp(d), is the operational quantity for individual monitoring: the dose equivalent in soft tissue (ICRU-sphere) below a specified point on the body at an appropriate depth d.

This quantity can be used for measurements of superficial and deep organ doses, depending on the chosen value of the depth in tissue. The depth d is expressed in millimeters, and ICRU recommends that any statement of personal dose equivalent should specify this depth. For superficial organs, depths of 0.07 mm for skin and3 mm for the lens of the eye are employed, and the personal dose equivalents for those depths are denoted by $H_p(0.07)$ and $H_p(3)$, respectively. For deep organs and the control of effective dose, a depth of 10 mm is frequently used, with the notation Hp(10).

The personal dose equivalent varies from person to person and from location to location on a person, because of different scattering and attenuation. However, Hp(d) can be assessed indirectly with a thin, tissue equivalent detector that is worn at the surface of the body and covered with an appropriate thickness of tissue equivalent material. ICRU recommends that dosimeters be calibrated under simplified conditions on an appropriate phantom[4,22].

II. 1.4. Dose Limits

Radiation dose limits represent the absolute maximum dose a person or organ can receive in a year. Dose limits are much lower than the threshold doses required for deterministic effects, so the aim of dose limits is to limit the risk of stochastic effects taking place. The unit of measurement for dose limits is the Sievert (Sv), which is the unit of dose equivalent [1, 6, 7].

Table(II.3):dose limits according to the recommendations of the ICRP[6].

Type of dose limits	worker (mSv/an)	Public (mSv/an)
Effective dose	20	1
Equivalent dose:		15
Crystalline	150	50
Skin	500	

II.2. Dosimeters of ionizing radiation

Radiation dosimetry is the process of determining the energy absorbed in a specified target from a radiation field. The processes by which energy is transferred from the radiation field and absorbed in the target tissue depend on the nature and energy of the radiation. It issued for the measurement of personal dose equivalents, or personal dose equivalent rates, kerma quantities required for radiation protection purposes as the exposition rate.

Two kinds of dosimeters are used: active or passive. The first device measures absorbed dose in real time, and the second gives integrated absorbed dose over a period of time [1, 25, 26].

II.2.1.Luminescence

A luminescing system is constantly expending energy to drive the emission process. The general thermluminescence includes a wide variety of light emitting processes which derive their names from the varied sources of energy that power them. Photoluminescence, which includes fluorescence and phosphorescence, is one among many luminescent categories. To illustrate the diversity of luminescence emissions[27, 28].

II.2.1.1. photoluminescence

Luminescence in solids is the phenomenon in which electronic states of solids are excited by some energy from an external source and the excited energy is released as light. When the energy comes from short wavelength light, usually ultraviolet light the phenomenon is called photoluminescence (PL).

II.2.1.2. Fluorescence

Is defined as a photoluminescent emission that arises from the singlet electronic state. To the human eye fluorescence is observed only when the exciting light source shines on the radiator [29, 30].

II.2.1.3.Phosphorescence

is defined as a photoluminescent process that originates from the triplet electronic state. Emissions from the triplet state are from 10 to 10,000 times longer than fluorescence; therefore, to the eye these radiators appear to emit after the excitation radiation is removed [27, 29, 30].

II.2.1.4. Radioluminescence

Radioluminescence is produced by ionizing radiations. Some polymers contain organic molecules which emit visible light when exposed to such radiations as X-rays, gamma rays or cosmic rays, and thus act as detectors for high energy radiations[30, 31].

II.2.2. Luminescence dosimeter

Some materials, known as luminescent detectors, when irradiated emit a quantity of light proportional to the absorbed ionizing radiation. Three groups of luminescence detectors are applied in personal dosimetry : Thermoluminescence detectors (TLD), Optically stimulated luminescent detectors (OSLDs) and radiophotoluminescent glass detectors (RPLGDs) [25, 31].

II.2.2. 1.The Mechanism of Luminescence

The electrons in orbit around an atom occupy a series of discrete energy levels. In a crystal, interactions between neighboring atoms result in these energy levels being broadened into a series of continuous energy bands. The highest filled band is called the valence band and it is separated from the conduction band by an energy gap of a few electron-volts. Electrons in the conduction band are free to move within that band. The energy gap separating the conduction and valence bands is sometimes referred to as the forbidden zone. If impurities are introduced into the crystal, intermediate energy levels are formed within the forbidden zone and these are referred to as electron traps. If the crystal is irradiated, electrons in the valence band may receive sufficient energy for them to be raised to the conduction band. Electrons may then fall back to the valence band or get caught in an electron trap (Figure II.2).

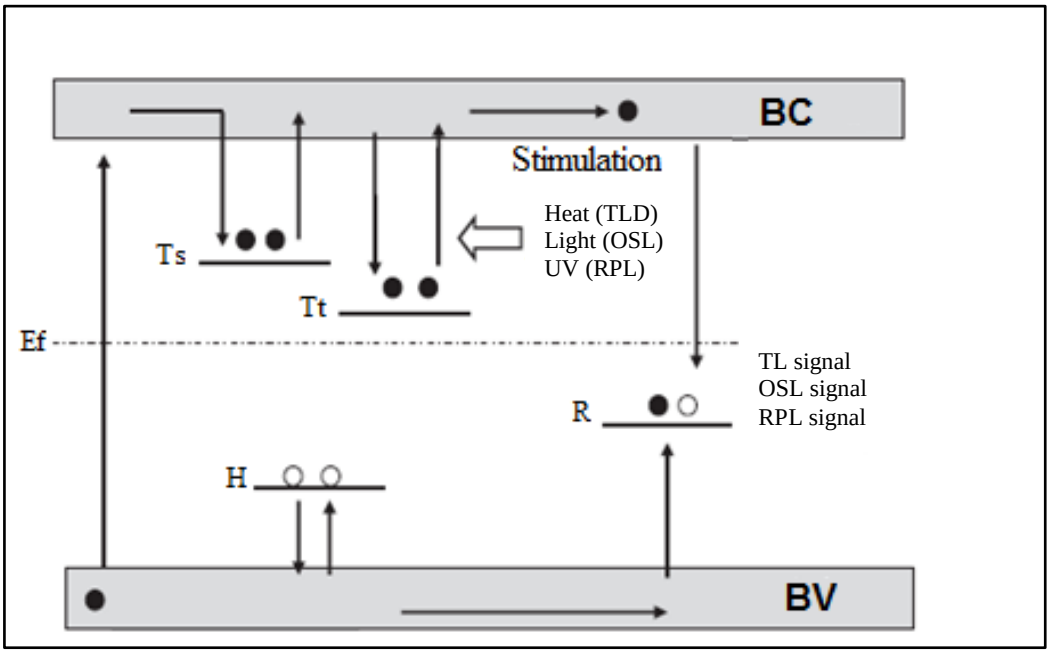

Figure(II.2): Basic principles of TL, OSL and RPL process[31].

Electrons caught in the traps are unable to escape until the crystal is like: heat, light, or Uv. When sufficient heat or light or Uv is applied the electrons gain thermal or light energy and fall back from the electron trap to the valence band; in doing so the electrons emit energy in the form of light photons. The total light output is proportional to the number of trapped electrons which in turn is proportional to the energy absorbed from the radiation beam [15, 29].

II.2.2.2. The type of dosimeter luminescence

II.2.2.2.1.Thermoluminescence dosimeter (TLD)

Thermoluminescence(TLD)is a temperature stimulated light emission from a crystal after removal of excitation, that the amount of light released by the phosphor material which has been exposed to ionizing radiation, will depend on the radiation dose received by the material and it is sensitive dosimeter. (TLDs) come in very small dimension sand their use, to a great extent, approximates a point measurement [3, 32].

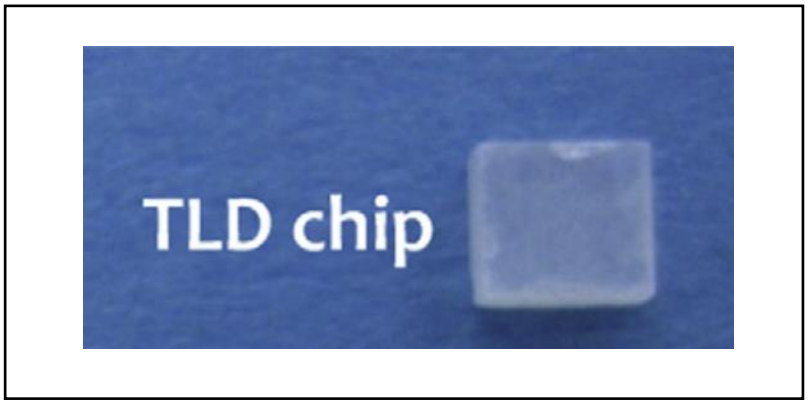

Figure(II.3): Thermoluminescence dosimeter [33].

II.2.2.2.2.Optically stimulated luminescent dosimeters (OSLDs)

Optically stimulated luminescent dosimeters (OSLDs) are becoming increasingly popular for measuring an absorbed dose in clinical radiotherapy.

OSLDs have known energy dependence, and this is accounted for by either calibrating the OSLD with a specific nominal energy, or using a standard energy correction factor to account for differences between the experimental beam photon energy and the photon energy used to establish the OSLD's sensitivity(giving large amounts of light output for relatively small absorbed doses). Carbon-doped aluminum oxide (Al_2O_3:C) has been used for some 15 years is the most commonly used OSLD material in the medical environment.

The underlying process by which energy is deposited and trapped in the crystal structure of Al2O3:Cis similar to that of thermoluminescent materials ; the difference is that, after excitation, the crystal is stimulated using visible light as opposed to heat[3, 34, 35].

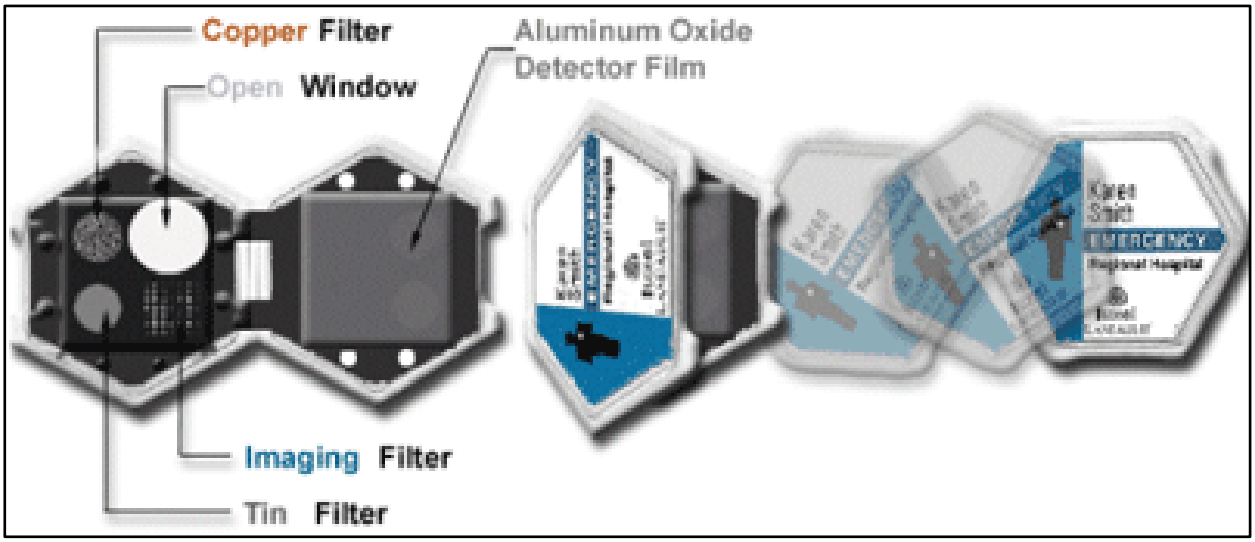

Figure(II.4): Optically stimulated luminescent dosimeter.

II.2.2.2.3.Radiophotoluminescence glass dosimeter

There is renewed current interest in the use of radiophotoluminescent glass dosimeters (RPLGDs), which were used by a few centers for radiotherapy applications in the 1950s and 60s, but not very widely since. Silver-activated phosphate glass (comprised of Ag^{+} and PO_4^{-3}ions), when irradiated, forms stable luminescence centers (Ag^{0}, Ag^{2+}), which are able to absorb and release energy. By illuminating the RPLGD with an ultraviolet laser, orange luminescent light is produced. Unlike the case in TLDs, the luminescence centers are not destroyed by the readout process, so the devices can be read out multiple times. Current systems use the difference in fluorescence decay times between surface contamination (0.3μs) and radiophotoluminescence (3.0μs) to discriminate signal from contamination noise, making handling easier….One complication with the use of RPLGDs is the fact that following irradiation, some electrons require additional energy to correctly enter luminescence centers, which can be supplied by heating, thus increasing the luminescence signal by up to 50% (sometimes termed the 'build-up effect')[3, 34].

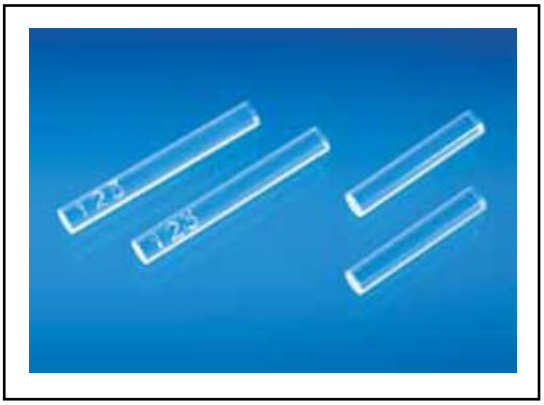

Figure(II.5):RPL dosimeters made of glass with a plastic capsule and tin filter[36].

II.3.Radiophotoluminescence glass dosimeter

II.3.1. Photosensitive glass

Photosensitive glass represents a very promising material for the effective fabrication of optoelectronic elements of very small dimensions. The illumination of the photosensitive glass by the light of appropriate energy results in the formation of "defects" usually possessing an unpaired electron. This causes a local increase of the refractive index. The Photosensitive glass depends on the phenomenon photoluminescence (PL)[37].

II.3.2.Radioluminescentsglass

Exposure to ionizing radiation induced a number of changes in the properties of glass doped argon. It can show a phenomenon of luminescent center which molecular act as of radiophotoluminescencecenter.

RPL is a phenomenon where a Ag-activatedphosphate glass emits a luminescence when excited with ultraviolet light after exposure to ionizing radiation[2].

II.3.3.Chemical characteristics of the silver ions

For centuries, silver has been used in medicinal applications[38]. The color centers were structured at the silver activated phosphate glass. The numbers of ionic silver relate to energy levels in color centers and the numbers of electron trap(s). The numbers of electron trap(s) increase with increasing numbers of ionic silvers. However, excessive numbers of ionic silver decrease the penetration efficiency of the pulse ultra-violet laser and increases energy dependence. Therefore, a proper ratio of ionic silver is required for the best luminescence and excitation efficiency[2, 39].

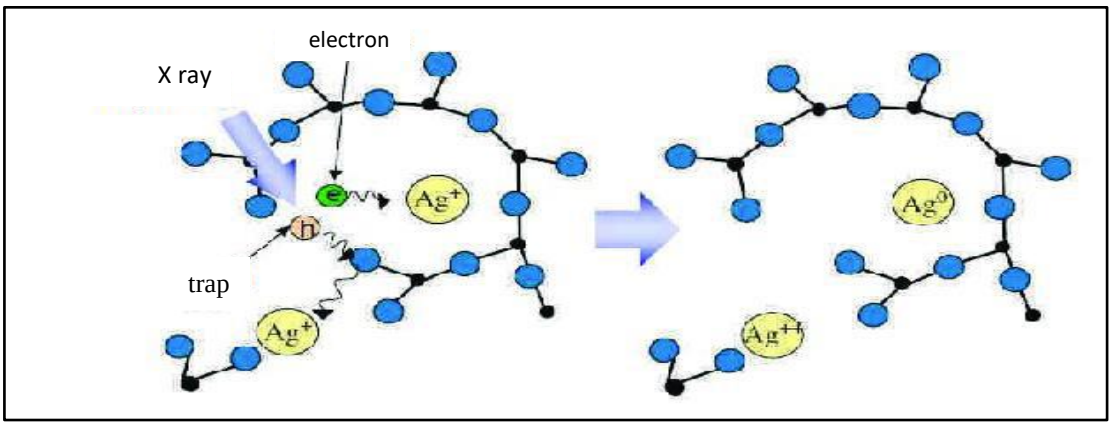

Figure(II.6): The color centers formation mechanism of FD-7 (A. T. G.).

II.3.3.1.LuminescentcentersinRPLDmaterial

RPLD material consists of a glass substrate incorporating ions of silver (Ag^{+}) and phosphate (PO_4^{3-}), The location of these ions represents defects in the lattice of the dosimeter material. Irradiation releases electrons in the dosimeter material; as a result, there are electron-hole pairs which are caught by Ag^{+} ion and PO_4^{3-} ion, creating stable luminescent centers (Ag^{0}, Ag^{++}) which are defined for the electron trap as:

$$Ag^{+} + e^{-} \longrightarrow Ag^{0}$$

and for the hole trap as:

$$Ag^{+} + hPO_4 \longrightarrow PO_4 + Ag^{++}$$

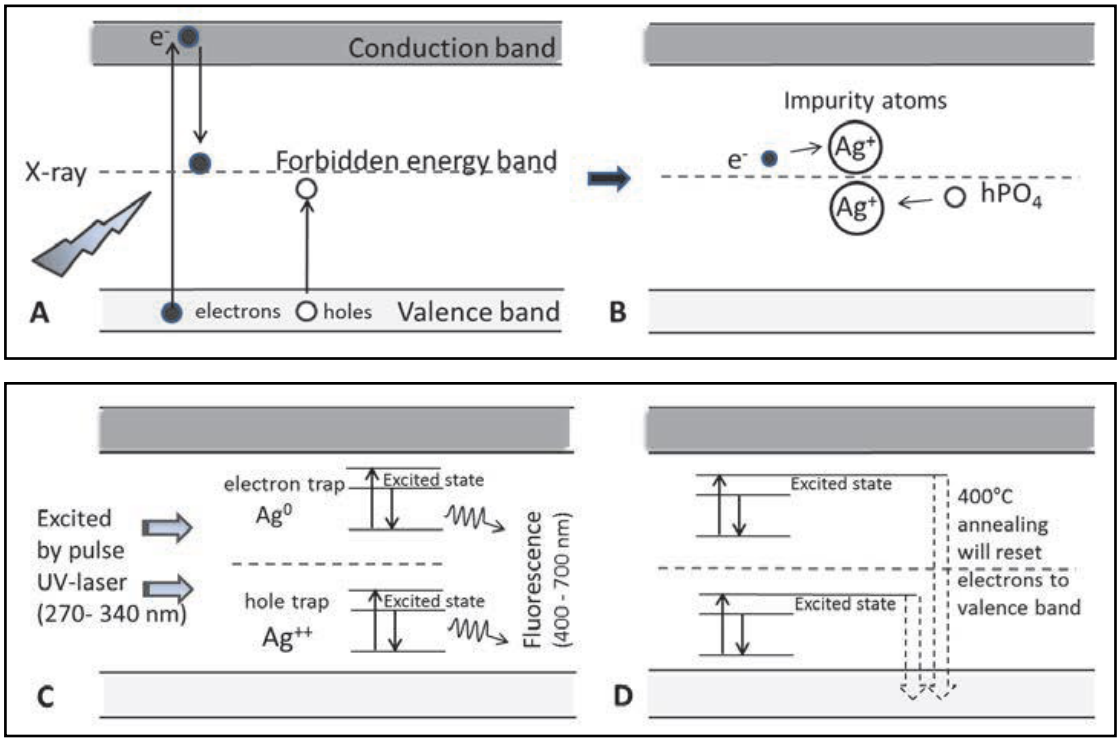

Figure(II.7): Schematic representation of creation of stable luminescent centers (Ag^0, Ag^{++}) by X-ray, C) fluorescence emission after UV excitation and D) annealing in 400°C to empty dosimeters[13].

The traps are stable in the sense that the energy required to remove the electron or hole from the trap to the conduction or valence band must be much larger than the binding energy of the electron in the trap. The electrons move slowly to the traps and dose fading is minimal. During the irradiation of the silver-activated phosphate glass, luminescent centers begin to form. However, the formation of these centers does not appear immediately, because some of the electrons are caught in effective traps which do not produce luminescence. After a ten- and hundred-day follow-up study at room temperature, 90% and 99% of the total dose of the dosimeter is reached, respectively. This phenomenon is known as the build-up effect and requires a stabilization treatment by heating in 70°C or 100°C. The electrons diffuse faster than holes in the glass material, and the accumulation speed of Ag^0 is thus higher than that of Ag^{++}. This build-up effect is stabilized by heating.

Stable luminescent centers are able to absorb and release energy; this is used as the principle in the dosimeter readout system. When the luminescent centers are irradiated by pulsed ultraviolet laser (270–340 nm), electrons are excited into a higher energy state. The centers return to a stable energy level by emitting light (420–700 nm) known as fluorescence. The fluorescence is

measured with a photomultiplier system, and the amount of fluorescence is directly proportional to the dose absorbed into the dosimeter. Figure(II.7) shows that [13, 40].

II.3.4.RPLD read-out device

Readout is a system for measuring a dose-dependent radiophotoluminescence (RPL) signal of a silver-activated phosphate glass dosimeter. The developments of new generation RPLGD and readout system were completed in 1990 [39]. The present reader consists of a modulated continuous-wave (cw) using pulsed UV-laser excitation and the dosimetric properties, such as energy and angular response, random uncertainty and ambient parameters affecting the dose measurement.

The actual progress in the field of photoluminescence dosimetry and thus the breakthrough of a so far unattractive technique is based on a modern evaluation technique using pulsed UV-laser excitation and a fully automatic readout [41].

The amount of orange light emitted from RPLGD is linearly proportional to the radiation received; therefore, it is suitable for long term personal dose monitor or environmental radiation monitor [39].

The reader unit is used to detect the intensity of the orange luminescence and converts this into personal dose equivalent[2, 35], in read-out system is contain also on holder, lock figure (II.8)

Figure(II.8): Automatic RPLD read-out device in the left and holder in the right [36].

II.3.5.Applications of RPLGD

- RPLGD can be used for small field radiationmeasurements effectively. Nose designed a tube to hold RPLGDs for dose measurements for head and neck patients to verify the delivery dose against the calculated dose from treatment planning system (Nose).

Although the maximum dose variation can be as high as 15%; however, those differences are mostly from the positioning errors. Based on the RPLGD physical characteristics study, the error from the RPLGD system stability is less than 3% (out of 15%) [39].

- Used for calculate : dose effect, rate dose, energy dependence and angular dependence.
- Used to detect radiation in a place or a person.
- Used in radiotherapy.
- Verification of delivered dose in radiotherapy and diagnostic imaging using phantom simulation.
- Studies using small animal irradiation experiments[36].

CHAPTER III

MONTE CARLO SIMULATION

CHAPTER III

MONTE CARLO SIMULATION

The name "Monte Carlo" was invented in the forties by scientists Working"Nicholas Metropolis and StanislasUlam" on the project of nuclear weapon in "Los Alamos " todesignate a class of numerical methods based on the use of numbers Random.

In this chapter, we shall see a generality for Monte Carlo method with the most important simulation codes, and a detail description of our simulation code MCNP5.

III.1.Monte Carlo Method

Monte Carlo techniques are a widely used class of computational algorithms for the purpose of statistically modeling various physical and mathematical phenomena [42].

Monte Carlo can be used to duplicate theoretically a statistical process (such as the interaction of nuclear particles with materials) and is particularly useful for complex problems that cannot be modeled by computer codes that use deterministic methods. The individual probabilistic events that comprise a process are simulated sequentially. The probability distributions governing these events are statistically sampled to describe the total phenomenon.

In general, the simulation is performed on a digital computer because the number of trials necessary to adequately describe the phenomenon is usually quite large. The statistical sampling process is based on the selection of random numbers analogous to throwing dice in a gambling casino — hence the name “Monte Carlo.” In particle transport, the Monte Carlo technique is pre-eminently realistic (a numerical experiment). It consists of actually following each of many particles from a source throughout its life to its death in some terminal category (absorption, escape….etc).

Probability distributions are randomly sampled using transport data to determine the outcome at each step of its life [43].

One of the most important issues limiting the use of Monte Carlo techniques for clinical absorbed dose calculations is the long execution time required to reduce the statistical variance associated with the calculated absorbed dose at each differential volume [42].

III.1.1. Random numbers

Random numbers have been used for more than 4,000 years. People use this numbers everywhere, in applications as simulations in mathematics ,fundamental physics….

In the Monte Carlo method, Random numbers are a key tool for. It is required to produce random numbers quickly when necessary, but to have access them use, we need a source of random numbers, this source called a random number generator (RNG) which is produced by algorithms[44,45, 46].

There are two principal methods used to generate random numbers. The first method known as true random number generators measures some physical phenomenon that is expected to be random and uses the measure to generate random number sequence. The second method known as pseudo random number generator uses computational algorithms that can produce long sequences of apparently random results, which are in fact completely determined by a shorter initial value, known as a seed value or key. The random number generator directly influences the accuracy of the simulation, it is based on the following recurrence formula [45,47,48] :

$$X_{n+1} = (a\,X_n + c) \bmod m \qquad \text{(III.1)}$$

where

$n \geq 0$ and $m > 0$.

m: the modulo m fait intervenir une division euclidienne de $(a\,X_n + c)$ par m.

X_0: the starting value, it is number used to produce a pseudo-random sequence called seed ($0 \leq X_0 < m$ a and c denote respectively the multiplier and the increment.

a : the multiplier; $0 \leq a < m$.

c: the increment; $0 \leq c < m$.

However, the periodicity of the sequence limits the validity of the random variable generator. It is therefore beneficial for this period to be very large. For this, we take:

$$c = 0 \text{ and } m = 2^N$$

where N is generally of the order of 30 or 40.

The numbers obtained have a uniform distribution. To obtain these numbers in the interval {0, 1}, we divide the X_i by (m-1) and obtain the following sampling relationship:

$$X_n = \frac{Xn}{m-1} = \frac{a}{m-1} X_{n-1} \quad \text{(III.2)}$$

III.1.2. Monte Carlo Method vs. Deterministic Method

Monte Carlo methods are very different from deterministic transport methods. Deterministic methods, the most common of which is the discrete ordinates method, solve the transport equation for the average particle behavior. By contrast, Monte Carlo obtains answers by simulating individual particles and recording some aspects (tallies) of their average behavior. Deterministic methods typically give fairly complete information (for example, flux) throughout the phase space of the problem. Monte Carlo supplies information only about specific tallies requested by the user. In the limit, this approaches the integro-differential transport equation, which has derivatives in space and time. By contrast, Monte Carlo transports particles between events (for example, collisions) that are separated in space and time [43].

Monte Carlo methods are usually requires a computer, by contrast, deterministic techniques It need not always be implemented on a computer – paper analyses may suffice, in Calculations Monte Carlo methods can take much longer than analytical models[49]. In the table below show Comparison between Monte Carlo methods and deterministic techniques.

Table(III.1): Comparison between Monte Carlo methods and deterministic techniques[42]:

Term	Deterministic	Monte Carlo
1. Geometry	Discrete/ Globally Discretized	Exact
2. Energy treatment-cross section	Discrete	Exact
3. Direction	Discrete/ Turncated series	Exact
4. Input preparation	Varies	Simple
5. Computer memory required	Large	Small/ Large
6. Computer time	Small	Large
7. Numerical issues	Convergence	Statistical uncertainty
8. Amount of information	Large	limited
9. Parallel computing	Complex	Trivial

III.1.3. Transport of particles

In this work, we focused mainly on the electron-matter interaction, when the passage of an electron in the middle of a physical interaction is called the Coulomb interaction and through the

collision the electron orbits of an electron or nucleus happen In both cases, the first electron loses energy and recorded death. Event tracking is done step by step and by order Chronology: sampling of the mean free path, sampling of cross sections Differential and total, the nature of the interaction, the direction and the loss of energy following the interaction, a process that begins again with the particles generated.

III.1.3.1.Transport of electrons

Unlike photons, electrons can interact several times with the medium of molecules in which crossed through it during the time, and because of this interaction is the impact mail as the transmission of this or these electrons have track lines broken and that is what is causing at the exit of electrons from the other side of the center of different energies completely,then move the electrons take a long time, which affects the way the Monte Carlo simulation, and it affects the dosimetry and irradiation account, so it must be used to maintain the simulation techniques[6].

III.2. Main Monte Carlo Simulation Codes

III.2.1. PENELOPE code

The PENELOPE code, issued by the University of Barcelona, is the most recent of the three mentioned in this article. The first official version dates back to 1996.

The PENELOPE code is recognized as one of the Codes with both numerical models and the most detailed and up-to-date sections in the processing of electron transport, in particular Low energies. For comparison, the two codes Precedents stop the individual monitoring of electrons that their kinetic energy is equal to 1 keV. This difference is related to the fact that this code was originally developed for the transport of electrons and extended to that of the photons. In addition, this code has a good ability to take complex geometries into account by combining of eleven basic quadratic surfaces. These Advantages are to be compared with the slowness of the calculations related to the detailed processing of particle transport Loaded and the current lack of a parallel version The code[46, 47, 50].

III.2.2.GEANT4code

GEANT4 is a Monte Carlo-based code, that is developed in two independent studies at CERN and KEK in 1993.Is based on a focused programming C ++ object[51].It allows to simulate the response function of the detector by Based on the different types of interactions. In-depth studies

can be carried out on any experiment taking into account the geometry of the experimental device, the materials Primary and secondary particles and their step-by-step follow-up Medium studies. GEANT4 is used in several branches of physics: physics of Particles, nuclear physics..[6].

III.2.3EGSnrccode

The EGS (Electron-Gamma-Shower)system of computer codes, is a general purpose package for the Monte Carlo simulation of the coupled transport of electrons and photons in an arbitrary geometry for particles[52].

III.2.4. MCNP code

The code MCNP(Monte Carlo N-Particle) developed and maintained by Los Alamos National Laboratory, primarily analyzes the particles neutrons, photons and electrons, uses continuous-energy nuclear and atomic data libraries[43]. The user creates an input file that is subsequently read by MCNP. This file contains information about the problem in areas such as: the geometry specification, the description of materials and selection of cross-section evaluations, the location and characteristics of the neutron, photon, or electron source, the type of answers or tallies desired, and any variance reduction techniques used to improve efficiency [53].

III.2.4.1.Units Used by MCNP

The units used by MCNP are (1) length in cm, (2) energy in MeV, (3) time in shakes (10^{-8} s), (4) temperature in MeV (kT), (5) atom density in atoms b^{-1} cm^{-1}, (6) mass density in $g.cm^{-3}$, and(7) cross sections in barns [53].

III.3. Description of MCNP5 code

MCNP5 code is a Monte Carlo-based simulation of particle transport and interactions with matter. MCNP5 is mostly used by nuclear engineers and scientist around the world for a vast number of research simulations. It has a wide range of applications in the fields of medical physics, reactor physics calculations, reactor safety calculations, and radiation dose estimates[51].It is necessary to define the cells, surfaces, materials, the parameters of the simulation and the type of answers desired.

III.3.1.Structure of the MCNP5 file

It contains an input file (the required algorithm) and the output file (contains all the measurements and the desired results on the issue of transmission or distribution of particle).The input file consists of three blocks [53, 54]:

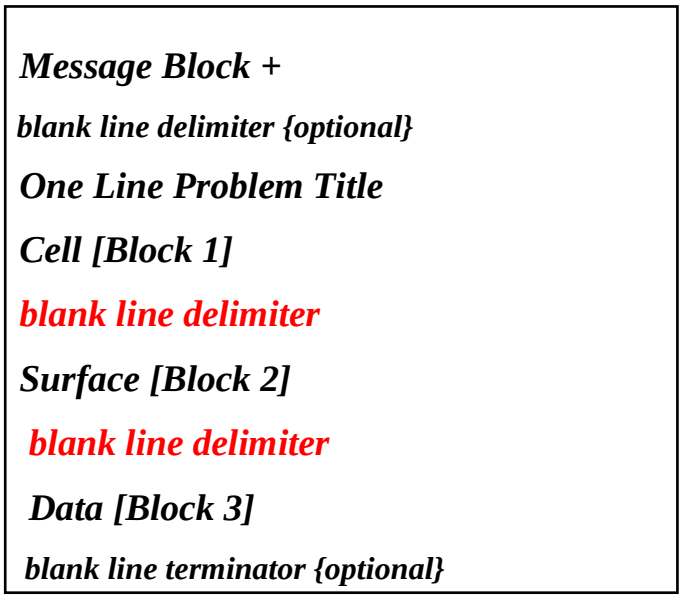

Figure (III.1) :MCNP input file structure.

III.3.2.Cells

Cells are defined as volumes of space bounded by surfaces, and it are used to define the shape and material content of the physical space of the problem. The cell is written by a number that defines the material constituting it and its density.

It has two meanings, one positive and the other negative. Applied to a closed surface, the sign (+)Indicates the outside of the cell and the (-) sign indicates the inside. The cell is the result of a Boolean logic(The intersection –and-, union – or-, complementarity of the different surfaces).The intersection is implicit and represented by the White between two surfaces is symbolized by( ). The union is given by (:). The last operator complementarity is symbolized by(#)which means everything (does not belong). The cell is declared in this form:

Figure (III.2) : Cell card format.

j :number of the cell given by the user.

m : number of the cell if it is not empty.

d : density of the material (atoms / cm^3) or g / cm^3.

geom: sign of the cell and the various Boolean operators quoted before.

params: optional, uses keywords like IMP, Vol, ...

III.3.3.Surface

The surface is the first element must be defined in the program, it used to create the geometry of a problem by applying logical operations and also use the cartesian coordinate system, mnemonic and equation. The specific format for a surface is shown in :

j a list

Figure (III.3): Surface card format.

j : represents the surface number.

a: represented the surface type (Coordinate transformations).

list: is a space for the user to list numbers that describe the surface. The predefined shapes are: SPH (sphere), RCC (cylinder), HEX (hexagon), and REC (cylinder Elliptic).In Table below are given the maps of surfaces recognized by the code.

Table (III.2): Library of surface maps recognized by MCNP [53, 55, 56].

Mnemonic	Type	Description	Equation	Card Entries
P	Plane	General	$Ax + By + Cz - D = 0$	*A B C D*
PX		Normal to x -axe	$x - D = 0$	*D*
PY		normal to y -axe	$y - D = 0$	*D*
PZ		normal to z -axe	$z - D = 0$	*D*
SO	Sphere	centered at origin	$x2 + y2 + z2 - R2 = 0$	R
S		general	$(x - \bar{x})2+(y - \bar{y})2+(z - \bar{z})2 - R2=0$	$\bar{x}\,\bar{y}\,\bar{z}$ R
SX		centered on *x*-axis	$(x - \bar{x})2+y2+z2 - R2 = 0$	$\bar{x}$ R
SY		centered on *y*-axis	$x2+(y - \bar{y})2+z2 - R2 = 0$	$\bar{y}$ R
SZ		centered on *z*-axis	$x2+y2+(z - \bar{z})2 - R2 = 0$	$\bar{z}$ R

C/X C/Y C/Z CX CZ	Cylinder	parallel to *x*-axis parallel to *y*-axis parallel to *z*-axis on *x*-axis on y-axis on z-axis	$(y-\bar{y})2+(z-\bar{z})2$ -*R2*=0 $(x-\bar{x})2+(z-\bar{z})2$ -*R2*=0 $(x-\bar{x})2+(y-\bar{y})2+$ -*R2*=0 $y2+z2-R2=0$ $x2+z2-R2=0$ $x2+y2-R2=0$	$\bar{z}$R $\bar{x}\bar{z}$R $\bar{x}\bar{y}$R R R R
K/X K/Y K/Z KX KY KZ	Cone	parallel to *x*-axis parallel to *y*-axis parallel to *z*-axis on *x*-axis on y-axis on z-axis	$\sqrt{(y-\bar{y})2+(z-\bar{z})2}$ -t$(x-\bar{x})$=0 $\sqrt{(x-\bar{x})2+(z-\bar{z})2}$ -t$(y-\bar{y})$=0 $\sqrt{(x-\bar{x})2+(y-\bar{y})2}$ -t$(z-\bar{z})$=0 $\sqrt{y2+z2}$ -t$(x-\bar{x})$=0 $\sqrt{x2+z2}$ -t$(y-\bar{y})$=0 $\sqrt{x2+y2}$ - t$(z-\bar{z})$=0	$\bar{x}\bar{y}\bar{z}$t2± 1 $\bar{x}\bar{y}\bar{z}$t2± 1 $\bar{x}\bar{y}\bar{z}$t2± 1 $\bar{x}$t2± 1 $\bar{y}$t2± 1 $\bar{z}$t2± 1
SQ	Ellipsoid Hyperboloid Paraboloid	axis parallel to *x*-, *y*-, or *z*-axis	±1 used only for 1-sheet cone $A(x-\bar{x})2+B(y-\bar{y})2+C(z-\bar{z})2+2D(x-\bar{x})+2E(y-\bar{y})+2F(z-\bar{z})+G=0$	A B C D E F G H J K
GQ	Cylinder, cone Ellipsoid Paraboloid Hyperboloid	Axis not parallel to *x*-, *y*-, or *z*-axis	$A_x{}^2+B_y{}^2+C_z{}^2+D_{xy}+E_{yz}+F_{zx}+G_z+H_y+J_z+K=0$	A B C D E F G $\bar{x}\bar{y}\bar{z}$
TX TY TZ	elliptical or circular torus. Axis is parallel to *x*-, *y*-, or *z*-axis	$(x-\bar{x})2/B2+(\sqrt{(y-\bar{y})2+(z-\bar{z})2}-A)2/C2-1=0$ $(y-\bar{y})2/B2+(\sqrt{(y-\bar{y})2+(z-\bar{z})2}-A)2/C2-1=0$ $(z-\bar{z})2/B2+(\sqrt{(x-\bar{x})2+(y-\bar{y})2}-A)2/C2-1=0$		$\bar{x}\bar{y}\bar{z}$ABC $\bar{x}\bar{y}\bar{z}$ABC $\bar{x}\bar{y}\bar{z}$ABC
XYZP	surfaces defined by points			

III.3.4.Definition of MCNP data

The format of the data card section is the same as the cell and surface card sections. The data card name must begin in columns 1-5. At least one blank must separate the data card name and the data entries. The most important data cards for medical physics applications include: problem type, source specification, tally specification, and material and cross section specification. These are only a few examples of the many available MCNP data cards.

The “MODE” card, discussed above, also serves as part of the source specification in some cases by implying the type of particle to be started from the source.

III.3.4.1.Sources

The source is defined by the SDEF card. This card is used once in an input file and can reproduce a large variety been sources. SDEF Card is one of four available methods of defining starting particles. The format for the source card is shown below in Figure (III.4)

SDEF source variable=specification…

Figure (III.4) : General source card format.

Within this source definition, the user can specify source distribution functions specified on “SIn (Source Information)”, “SPn (Source Probability)”, “SBn(Source Bias)”,and “DSn (n is the distribution number)” cards.

SInoption I1...Ik

SPnoption P1 ... Pk(orSPnf a b)

SBnoption B1 ... Bk(or SBnf a b)

Figure (III.5) : Sourcedistribution functions cards format.

The most common source variables used for “SDEF” specification are listed below in Table

(III.3)

Table (III.3) : Most common variables used for general source (“SDEF”) specification.

Variable	Meaning
ERG	Energy of the particle (MeV)
CEL	Source cell
SUR	Surface (Default case : Zero, means cell source)
RAD	Radial distance of the position
POS	Reference point for position sampling
PAR	Particle type source will emit
AXS	Reference vector for EXT and RAD
EXT	Cell case: distance from POS along AXS
	Surface case: cosine of angle from AXS
TME	Time when the particle started (shakes)
UUU, VVV, WWW	Direction of the flight of the particle
XXX, YYY, ZZZ	Position of the particle
WGT	Particle weight

III.3.4.2.Tallies

The tally cards are used to specify what you want to learn from the Monte Carlo calculation, perhaps current across a surface, flux at a point, etc. You request this information with one or more tally cards. Tally specification cards are not required, but if none is supplied, no tallies will be printed when the problem is run and a warning message is issued. Many of the tally specification cards describe tally “bins.” A few examples are energy (En), time (Tn), and cosine (Cn) cards. MCNP provides six standard neutron, six standard photon, and four standard electron tallies, all normalized to be per starting particle. Some tallies in criticality calculations are normalized differently.

The tallies are identified by tally type and particle type. Tallies are given the numbers 1, 2, 4, 5, 6, 7, 8, or increments of 10 thereof, and are given the particle designator :N or :P or :E (or :N,P only in the case of tally type 6 or P,E only for tally type 8). Having both an F1:N card and an F1:P card in the same INP file is not allowed. The tally number may not exceed three digits.

For our sample problem we will use Fn cards (Tally type) and En cards (Tally energy)[46, 53, 54, 57].

Table (III.4):MCNP tally commands and their corresponding units[57].

Mnemonic	Tally Description	Description	∗Fn units
F1:N or F1:P or F1:E	Current integrated over a surface	particles	MeV
F2:N or F2:P or F2:E	Flux averaged over a surface	particles/cm^2	MeV/cm^2
F4:N or F4:P or F4:E	Flux averaged over a cell	particles/cm^2	MeV/cm^2
F5a:N or F5a:P	Flux at a point or ring detector	particles/cm2	MeV/cm2
F6:N or F6:N,P or F6:P	Energy deposition averaged over a cell	MeV/g	MeV
F8:P or F8:E or F8:P,E	Energy distribution of pulses in a detector	pulses	jerks/g

III.3.4.3.Materials

The format of the material, or m card, in this section specifies both the isotopic composition of the materials and the cross section evaluations to be used in the cells. The material card is shown below in Figure (III.6).

mnzaid1 fraction1 zaid2 fraction2 …

mn = Material card name (m) followed immediately by the material number (n) on the card. The mn cards starts in columns 1-5.

zaid = Atomic number followed by the atomic mass of the isotope. Preferably(optionally) followed by the data library extension, in the form of .##L (period, two digits, one letter).

fraction = Nuclide fraction

(+) Atom density (atoms/b-cm)

(-) Weight fraction

Figure (III.6): Material card format.

The "*n*" on a material card corresponds to the material number on the cell card. The consecutive pairs of entries on the material card consist of the identification number (ZAID) of the constituent element or nuclide followed by the atomic fraction (or weight fraction if entered as a

negative number) of that element or nuclide, until all the elements and nuclides needed to define the material have been listed.

One simulation in MCNP uses one nuclear data library for every isotope specified in the MCNP input file. The selection of libraries is done through a unique identifier for each library, called ZAID(*ZZZAAA.nnx)*. These identifiers consist of the atomic number (Z), mass number (A) and library specified ID.

In calculations involving photons and electrons, the isotopes of the elements play the same role as natural elements; Consequently, the A's can be set to 0 and the numbers *nnx* forgotten. The fractional i numbers are the atomic fractions of component i or density atomic if introduced with a minus sign[53,56].

CHAPTER IV

CALCULATION OF ENERGY RESPONSE AND PERCENTAGE DEPTH DOSE

CHAPTER IV
CALCULATION OF ENERGY RESPONSE AND PERCENTAGE DEPTH DOSE

This chapter is devoted to the Monte Carlo simulation of energy dependence and the Percentage Depth Dose (PDD), where we cited the methods and materials these we used, and show obtained results with their discussion in the current work.

IV.1.Dosimetric system

IV.1.1.Dosimeters

In our study, we used two dosimeters radiophotoluminescence (RPL), the model GD- 450 and model GD- 302 without filter that are manufactured by" AGC techno Glass Corp.., Shizuoka, Japan". The dosimeter GD- 450 is 8 cm of diameter and 1mm of thickness, the dosimeter GD-302 is 1.5 mm of diameter and 12 mm of long. The both dosimeters are RPL FD-7 glass series. The weight compositions the FD- 7 glass series are: 31.5% P, 51.16% O, 6. 12% Al, 11.00% Na and 0.17% Ag, their effective atomic number Z_eff is 12.04 and its density ρ is 2.61 g.cm-3.[5, 39,58].

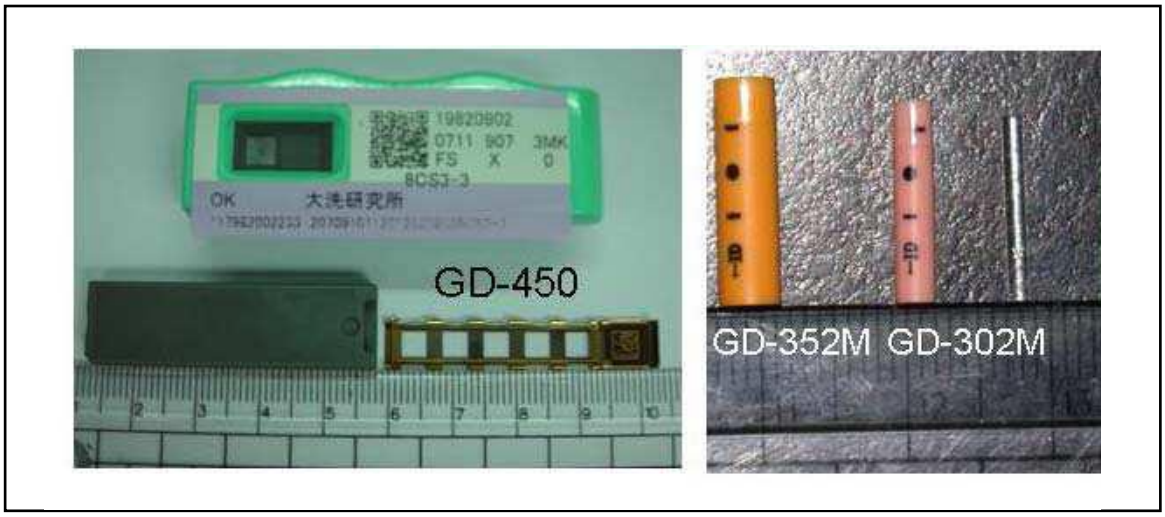

Figure (IV.1): Picture of radiophotoluminescence glass dosimeters RPL GD-450, GD-352 and GD-302 [39].

IV.1.2. Used phantom

The phantom material was water (H_2O), with sufficient material around the dosimeter to ensure full scatter conditions. The atomic compositions and density of the materials are listed in Table (IV.1). The water phantom whose polymethylmethacrylate (PMMA) walls were 10 mm thick (except along the beam axis where they were 2.5 mm thick)[59].

Each dosimeter is irradiated in a depth Z of the Phantom, the compositions atomic matters are listed in the Table (IV.1).

Table (IV.1): Phantom characteristics, weight compositions and density used in simulation MCNP5[29].

Element	Water	PolymethylMethacrylate(PMMA)
H	0.1119	0.0805
C	–	0.5999
O	0.8881	0.3196
Density(g/cm^3)	1.00	1.19
Z_{eff}	6.6	5.85

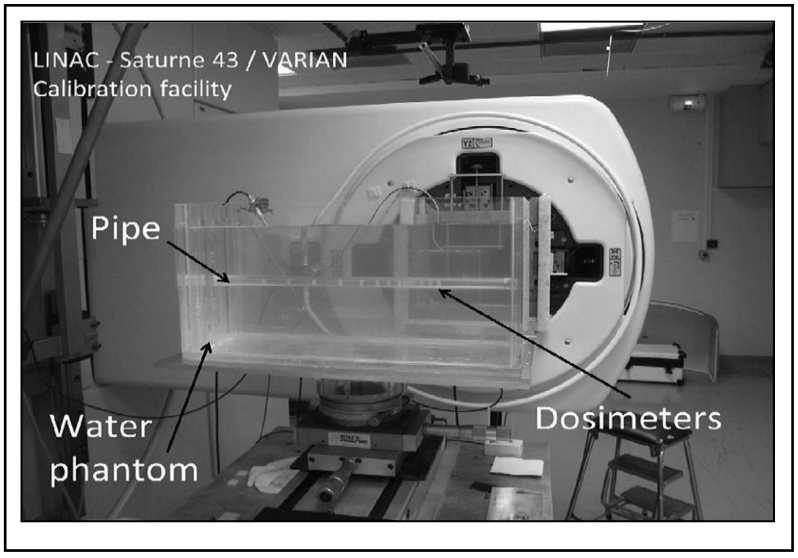

Figure (IV.2): Experimental example identical of our simulation study[60].

IV.2 Simulation Monte Carlo

In our work, we used the Monte Carlo simulation code MCNP version 5 (LANL 2003), as a means to calculate the answer of dosimeters such as energy response and Percentage Depth Dose (PDD). the MCNP5 with ENDF/B-VI cross section data was used in this study. In each radiophoto-luminescent detector, the code of particles transport MCNP5 was used to calculate

the deposed energy. The simulation is applied for a point electrons source collimated in a cone whose circular surface end equal to field sizes of electrons beam used.

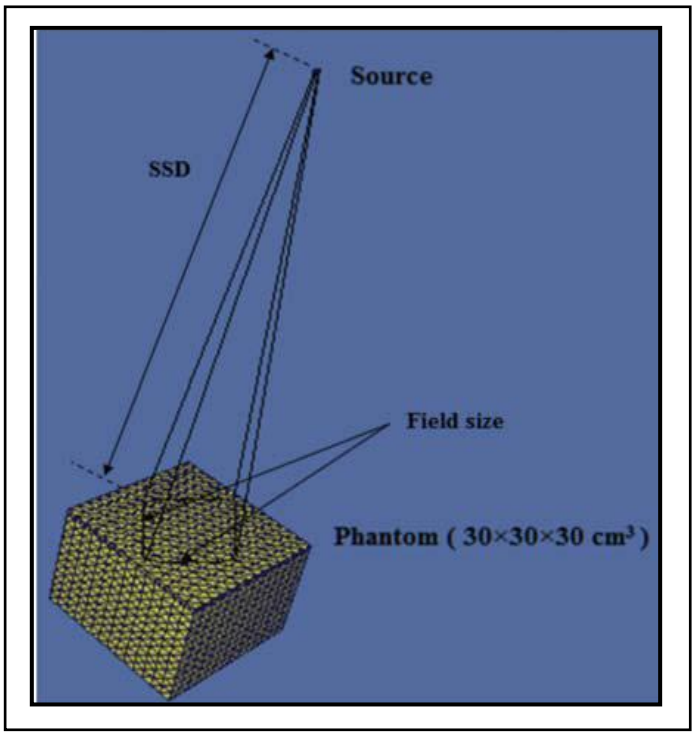

Figure (IV.3): Set up of the simulation study[61].

The luminescent dosimeters irradiated by a conical electron beam in a depth Z from the surface of the phantom. Figure (IV.3) gives the model of the installation used to the simulation of Monte Carlo.

The energy deposition in each dosimeter studied is calculated by using the Tally '*F8' of MCNP5 with particle transport mode "Mode :p e". To make all statistical checks recommended by MCNP5 code, the simulations are executed with a number of history of 100 million for each orientation, where reported that the relative error less than 2% was obtained for each simple calculation mentioned.

Calculations were carried out using the source-to-surface distance (SSD) of 100 cm with a field size of 15×15 $cm^2$for the clinical electrons beams, and 10x10 cm^2 for the^{60}Co photons beam. [5]

IV.3. Equivalent field and electron beams quality

Beams used in radiotherapy, have different forms which represent usually a compromise between the present form of the target and the need for simplicity and effectiveness in the formation of the beam. Four forms of field are used: square, rectangular, circular, irregular.

For our study, we used the field square arbitrary will be equivalent to a field circular with the radius$\boldsymbol{r_{eq}}$, where the two field have the same surface [1].

$$a_{eq}^2 = \pi r_{eq}^2 \quad \text{(IV.1)}$$

Where

$$r_{eq} = \frac{a_{eq}}{\sqrt{\pi}} \quad \text{(IV.2)}$$

The beam quality for electrons beam dosimetry is specified by R_{50}, the depth in water (in centimeter) at which the percent depth dose is 50% for a broad beam at an SSD of 100 cm, R_{50} for a broad beam may be determined by measurement (or calculation) of dose at two points on central axis: one at d_{max} and the other at depth where the dose falls to 50% of the maximum dose. The depth of 50% ionization (I_{50}) is determined by subtracting $0.5r_{cav}$ from the depth indicated by the center of chamber cavity. The beam quality specified, R_{50}, is then calculated from I_{50}[15, 62, 63] :

$$R_{50} = I_{50} - 0.06\text{cm} \quad [\text{for } 2 \leq I_{50} \leq 10 \text{ cm }] \quad \text{(IV.3)}$$

$$R_{50} = I_{50} - 0.37\text{cm} \quad [\text{for } I_{50} > 10\text{cm}] \quad \text{(IV.4)}$$

$$Z_{ref} = 0.6R_{50} - 0.1 \text{ cm} \quad \text{(IV.5)}$$

Z_{ref} : were set up on the reference depths in the water phantom for each electron beam energy to decrease the fluctuation error [6, 62].

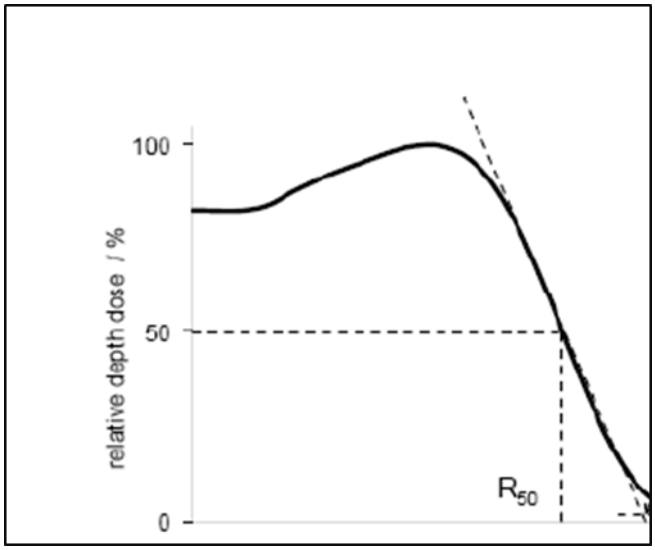

Figure (IV.4): schema determine R_{50}[17].

The below table illustrates the values of reference depth Z_{ref} according to energies beams (4-20 MeV) .

Table (IV.2): Physical parameters of clinical electron beams used in this study[64].

Electron beam energy (MeV)	**Z_{ref} (cm)**
4	0.9
6	1.4
9	2
12	2.8
16	3.8
20	4.9

IV.4. Percentage Depth Dose (PDD)

The electron beams in the energy range of 4-20 MeV are widely used in radiotherapy [65]. So, it is necessary to determine and use the dose data in depth for electron beams [66, 67].

Percent depth dose (PDD) is the ratio of absorbed dose (on the central axis) at a chosen depth to the absorbed dose at the reference depth D_{max} , so the relationship of Percentage Depth Dose is:

$$P = \frac{D_d}{D_{d_0}} \times 100 \qquad \text{(IV.6)}$$

where: **d** is any depth and $\mathbf{d_0}$ ($d_0=D_{max}$) is reference depth of maximum dose [6].

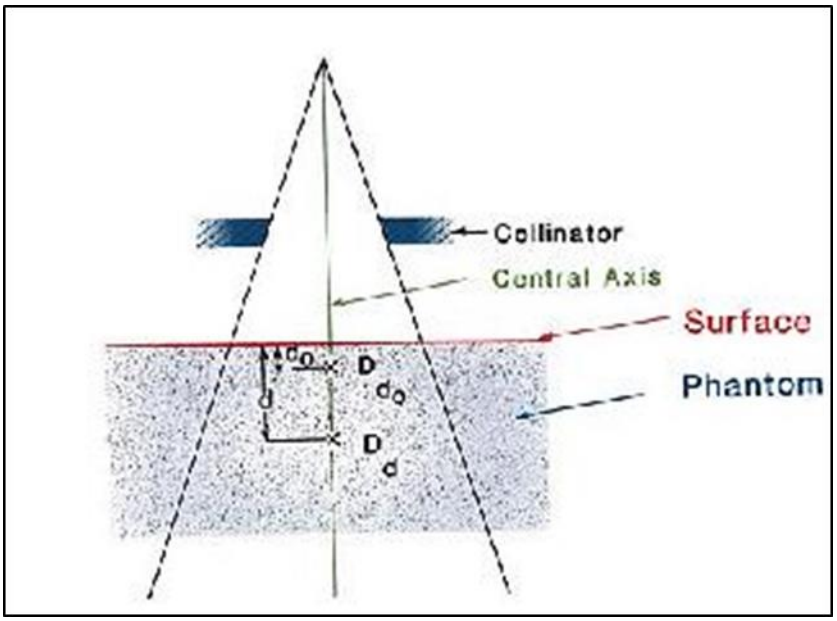

Figure (IV.5): schema determine Percentage Depth Dose[6].

Electron fields are most often used clinically with fixed SSD techniques. Only occasionally are is acentric techniques used. This section will deal with only fixed SSD dosimetry. Percent depth-dose calculations for electron beams should be performed for each available energy for the range of field sizes available. Small differences in energy, scattering foils, or scanning systems can affect the electron-beam characteristics [68, 69].

Table (IV.3): Monte Carlo calculated Percentage Depth Dose (PDD) for RPL GD- 450 with 4 MeV and 6 MeV electrons beams.

RPL GD- 450			
4MeV		**6MeV**	
Depth (cm)	**PDD (%)**	**Depth (cm)**	**PDD (%)**
0.4	84.909	0.9	89.3516
0.5	90.327	1	92.428
0.6	95.312	1.1	95.1996
0.7	98.673	1.2	97.504
0.8	100	1.3	99.175
0.9	99.110	1.4	100
1	95.776	1.5	99.864
1.1	89.801	1.6	98.657

1.2	80.911	1.7	96.226
1.3	68.947	1.8	92.498
1.4	54.046	1.9	87.405

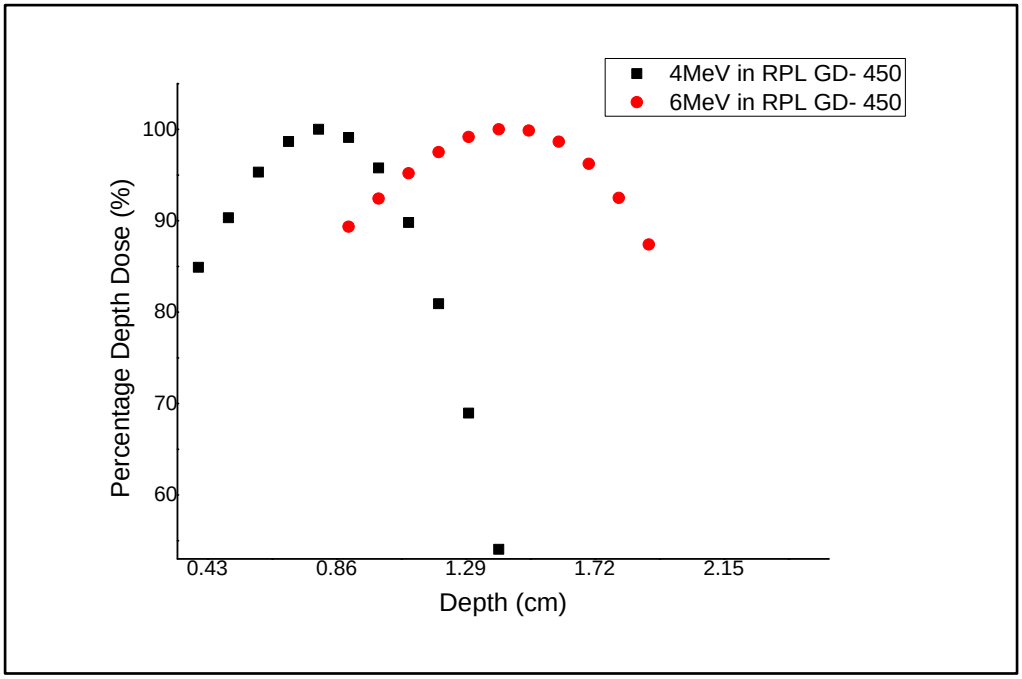

Figure (IV.6): Monte Carlo simulated Percentage Depth Dose (PDD) with 4 MeV and 6 MeV electrons beams forRPL GD- 450 (SSD= 100 cm, field size= 15 x15 cm^2).

Table (IV.4): Monte Carlo calculated Percentage Depth Dose (PDD) for RPL GD- 302 with 4 MeV and 6 MeV electrons beams.

RPLGD- 302			
4MeV		**6MeV**	
Depth (cm)	**PDD (%)**	**Depth (cm)**	**PDD (%)**
0.4	82.479	0.9	88.533
0.5	87.908	1	91.645
0.6	93.384	1.1	94.139
0.7	96.943	1.2	96.963
0.8	99.835	1.3	99.088
0.9	100	1.4	99.620
1	98.0545	1.5	100
1.1	92.866	1.6	99.302

1.2	83.916	1.7	97.225
1.3	71.963	1.8	93.892
1.4	57.161	1.9	89.008

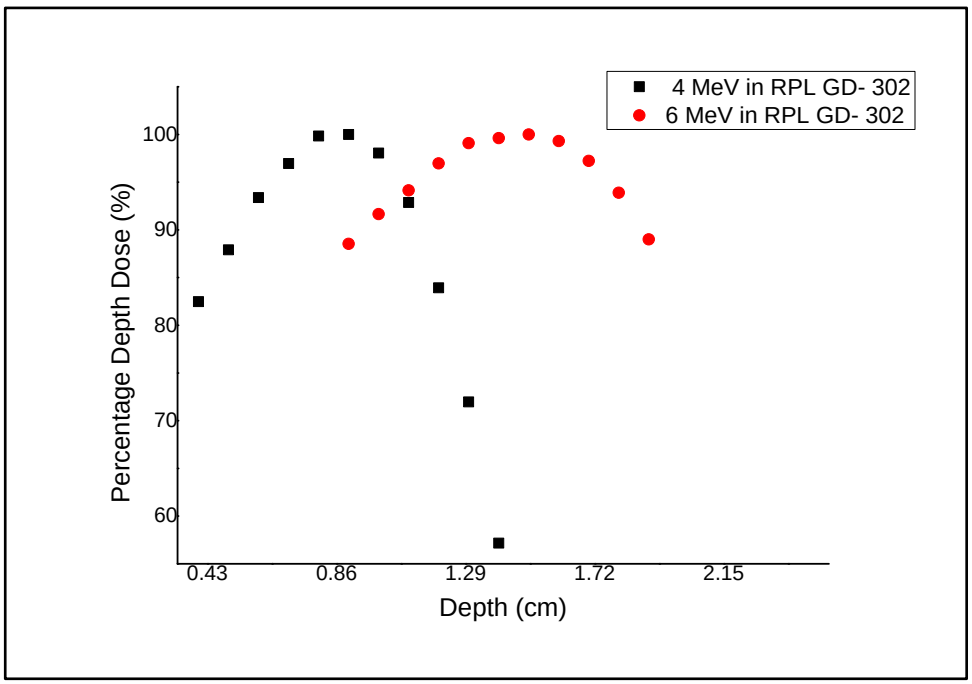

Figure (IV.7): Monte Carlo simulated Percentage Depth Dose (PDD) with 4 MeV and 6 MeV electrons beams for RPL GD- 302 (SSD= 100 cm, field size= 15 x15 cm^2).

Table (IV.5): Monte Carlo calculated Percentage Depth Dose (PDD) for water with 4 MeV and 6 MeV electrons beams.

Water			
4MeV		**6 MeV**	
Depth	**PDD (%)**	**Depth**	**PDD (%)**
0.4	81.122	0.9	87.651
0.5	86.033	1	90.806
0.6	92.196	1.1	93.389
0.7	96.357	1.2	95.903
0.8	99.550	1.3	98.094
0.9	100	1.4	99.037
1	98.612	1.5	100
1.1	94.49	1.6	99.404
1.2	86.88	1.7	97.975
1.3	77.050	1.8	94.534

1.4	65.001	1.9	89.960

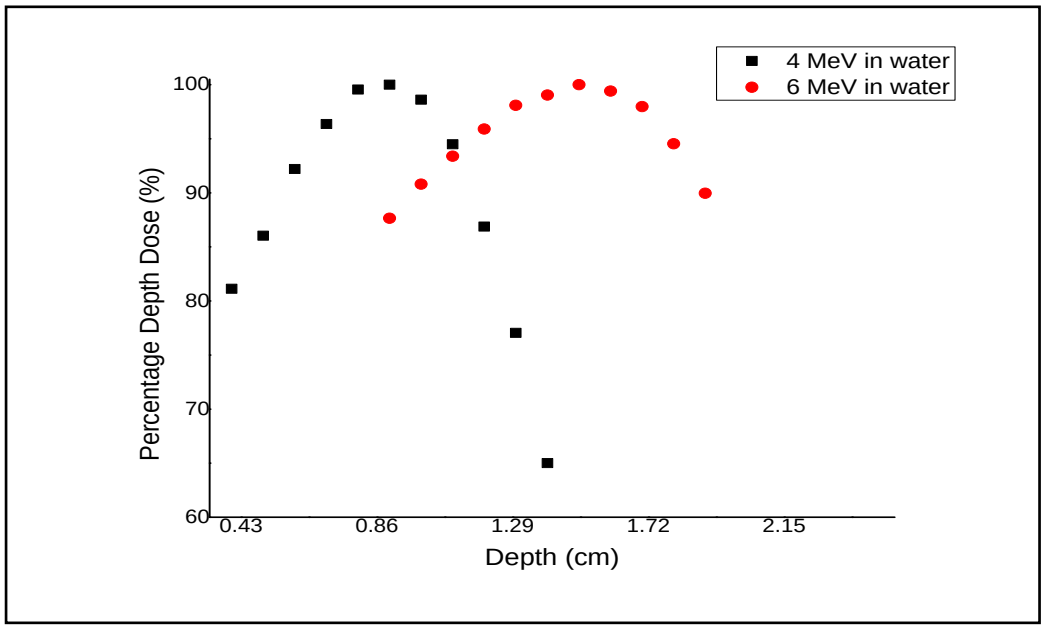

Figure (IV.8): Monte Carlo simulated Percentage Depth Dose (PDD) with 4 MeV and 6 MeV electrons beams for water (SSD= 100 cm, field size= 15 x15 cm^2).

For 4 MeV electrons beam, we found that the depth maximum dose was at depth Z=0.8 cm for RPLGD- 302 and water, for RPLGD- 450 the depth maximum dose was at depth of 0.9 cm.

For 6 MeV electrons beam, the results show that the maximum depth dose was at depth of 1.4 cm for RPLGD- 450, at depth of 1.5 cm for RPLGD- 302, and at depth of 1.5 cm for water.

The difference between the value of RPL GD- 450 and RPL GD- 302 is due to the difference of geometry, where the diameters are 8 mm and 1.5 mm for RPLGD- 450 and RPLGD- 302, respectively.

Our results confirm that, for constant field size and source surface distance (SSD) the PDD beyond Z_{max} increases with beam energy because of a decrease in beam attenuation (i.e. because of an increase in beam penetrating power)

In the same way, we can determine the depth of maximum dose for the rest energies of electrons beam 9, 12, 16 and 20 MeV.

IV.5. Energy dependence and quality correction factors

Absorbed dose at a reference depth Z_{ref} in water for a beam quality Q is given by the following equation [6]:

$$D_{W,Q} = M_Q \times N_{D,W,Q0} \times k_{Q,Q_0} \quad \text{(IV.7)}$$

Where:

$D_{W,Q}$ is the absorbed dose to water for a beam of quality Q, M_Q is the dosimeter reading adjusted influence other factors than those related to beam (pressure and temperature) and $N_{D,W,Q0}$ is the dosimeter calibration factor. in this work we used γrays of Cobalt-60 as the quality Q_0(reference beam) [7].

$$k_{Q,Q_0} = \left(F_{Q,Q_0}\right)^{-1} \quad \text{(IV.8)}$$

$k_{Q,Q_0}$is the correction factor to take account of the difference between the response of the dosimeter in beams of different qualities Q and Q_0 [64].

$$F_{Q,Q_0} = \frac{(r/D_W)_Q}{(r/D_W)_{Q_0}} = \frac{(r/D_{dos})_Q (D_{dos}/D_W)_Q}{(r/D_{dos})_{Q_0} (D_{dos}/D_W)_{Q_0}} \quad \text{(IV.9)}$$

Where:

$(r/D_W)_Q$is the dosimeter readingper dose to water at beam Quality Q, to obtain a dose reading linear. $(r/D_{dos})_Q$is corresponding reading per dose to the dosimeter and $(r/D_{dos})_{Q_0}$the ratio between the dose to the dosimeter and the dose to water.

You can set the energy dependence F_{Q,Q_0} according to the formula (IV.9):

$$F_{Q,Q_0} = G_{Q,Q_0} \times H_{Q,Q_0} \quad \text{(IV.10)}$$

Where :

$G_{Q,Q_0}$is called the relative effectiveness (or performance of radiation relative) of the dosimeter, and it's given by formulated:

$$G_{Q,Q_0} = \frac{(r/D_{dos})_Q}{(r/D_{dos})_{Q_0}} \quad \text{(IV.11)}$$

$H_{Q,Q_0}$is the report of the absorbed dose D_{dos} in the dosimeter per the absorbed dose in water D_W (without the presence of the dosimeter) for a beam quality Q with the absorbed dose D_{dos} in

the dosimeter per the absorbed dose in water D_W for a beam quality Q_0, $H_{Q,Q_0}$is given by an equation:

$$H_{Q,Q_0} = \frac{(D_{dos}/D_W)_Q}{(D_{dos}/D_W)_{Q_0}} \quad \text{(IV.12)}$$

Thus, for a performance constant radicals by absorbed dose to dosimeter (that is, when G_{Q,Q_0}equal the unit or one), F_{Q,Q_0}equal H_{Q,Q_0}. This factor is calculated by simulation of Monte Carlo in this work for beams energy high electron clinical .

The response of a dosimetry system is generally a function of radiation beam quality (energy). Since the dosimetry systems are calibrated at a specified radiation beam quality (or qualities) and used over a much wider energy range, the variation of the response of a dosimetry system with radiation quality (called energy dependence) requires correction[6].

The objective of this part of work is studying the energy response of two dosimeters GD-450 and GD- 302 for electrons beams, we used Monte Carlo simulation to calculate the energy response F_{Q,Q_0} for clinical electrons beam at the depths of 0.9, 1.4, 2.0, 2.8, 3.8 and 4.9 cm for the energy of 4, 6, 9, 12, 16 and 20 MeV, respectively, under the same conditions of irradiation. Through the relationship (II.14) and (IV.12), Thus, for a constant yield of radicals per absorbed dose to the dosimeter (that is, when $G_{Q,Q0}$ equals unity) [64], we can conclude:

$$F_{Q,Q_0} = H_{Q,Q_0} \quad \text{(IV.13)}$$

The results of the Monte Carlo simulations are displayed in Tables (IV.5 and IV.6), reported the energy response of the RPL dosimeters for clinical electrons, both RPLGD- 450 and RPLGD-302 (without filter)relative to ^{60}Co.

Table (IV.6): Monte Carlo calculated energy response $H_{Q,Q0}$for RPL GD- 450 irradiated with energy clinical electrons beam.

Beam quality		Depth (cm)	$H_{Q,Q0}$ RPL GD-450	$k_{Q,Q0}$ RPL GD-450
Reference : Rayon γ ^{60}Co		5	1	1
Clinicalelectrons	R_{50} (g/cm^2)			
4 MeV	1.333	0,9	0.968	1.033
6 MeV	2.167	1,4	0.968	1.033
9 MeV	3.167	2	0.948	1.055
12 MeV	4.5	2,8	0.932	1.073
16 MeV	6.167	3,8	0.922	1.085
20 MeV	8	4,9	0.920	1.087

Table (IV.7): Monte Carlo calculated energy response $H_{Q,Q0}$for RPL GD- 302 irradiated with energy clinical electrons beam.

Beamquality		Depth (cm)	$H_{Q,Q0}$ RPL GD-302	$k_{Q,Q0}$ RPL GD-302
Reference : Rayon γ ^{60}Co		5	1	1
Clinicalelectrons	R_{50} (g/cm^2)			
4 MeV	1.333	0,9	0.976	1.025
6 MeV	2.167	1,4	0.975	1.026
9 MeV	3.167	2	0.971	1.03
12 MeV	4.5	2,8	0.965	1.037
16 MeV	6.167	3,8	0.957	1.046
20 MeV	8	4,9	0.957	1.045

The interaction electrons beam with matter has two type: interactions of electron–orbital electron and interactions of electron –nucleus. Also use of gamma ray(^{60}Co) as reference ray(E=1.25 MeV).

Figure IV.9, illustrate results from the Monte Carlo simulation energy response of RPL GD-302 and GD-450 dosimeters calculated for clinical electrons beams compared with previous work.

The results show that, energy dependence F_{Q,Q_0} is decreases with increase of energy. According to this study, energies responses of 4 - 20 MeV electrons beams were approximately between 2.5% and 4.3% for RPLGD-302 ,and between 3.3% and 8% for RPLGD-450.

Thus, a correction factor should be determined for high energy electron beams used in evaluations, assessments, or for absorbed dose determination. Glass Dosimeters RPLGD- 450 and RPLGD- 302 were found to be suitable for dosimetry of high-energy electrons beams in the radiotherapy field.

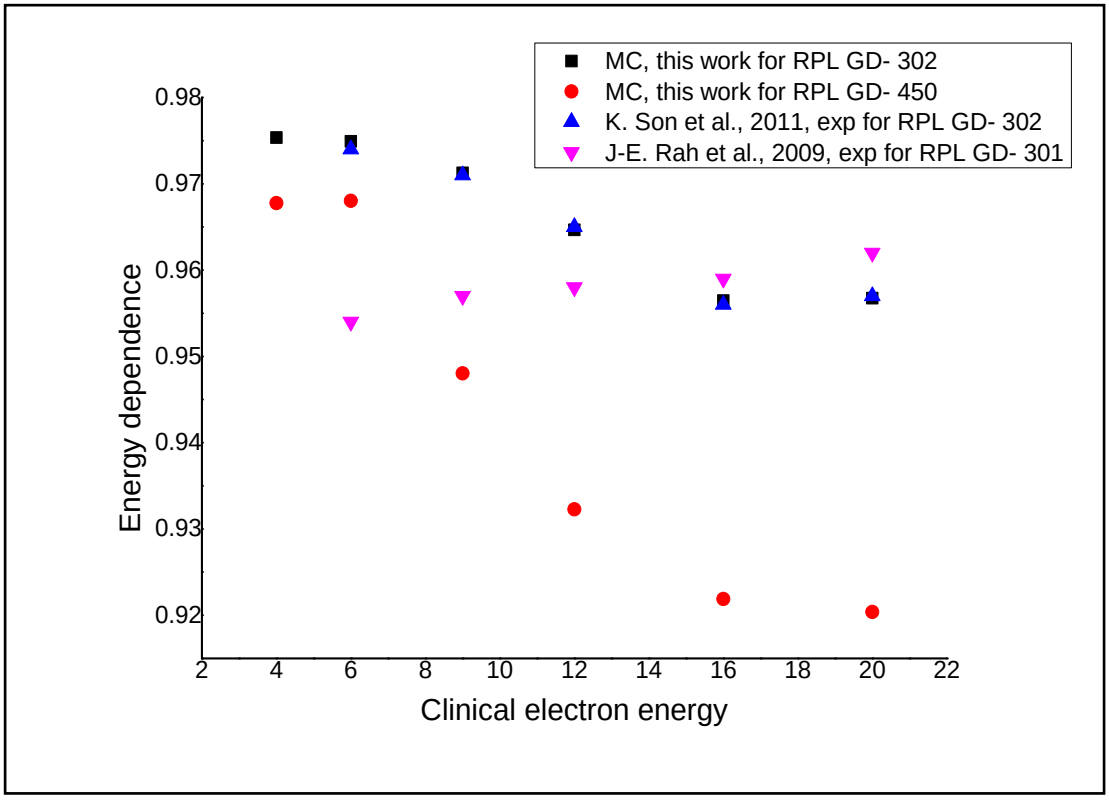

Figure (IV.9): Comparison between our work for RPL GD-302 And RPL GD-450 with the literature[5, 70].

The Monte Carlo calculations appear an over responses for both RPLGD- 450 and RPLGD- 302 appeared slow fall, by a maximum of 8 % and 4.3% respectively.

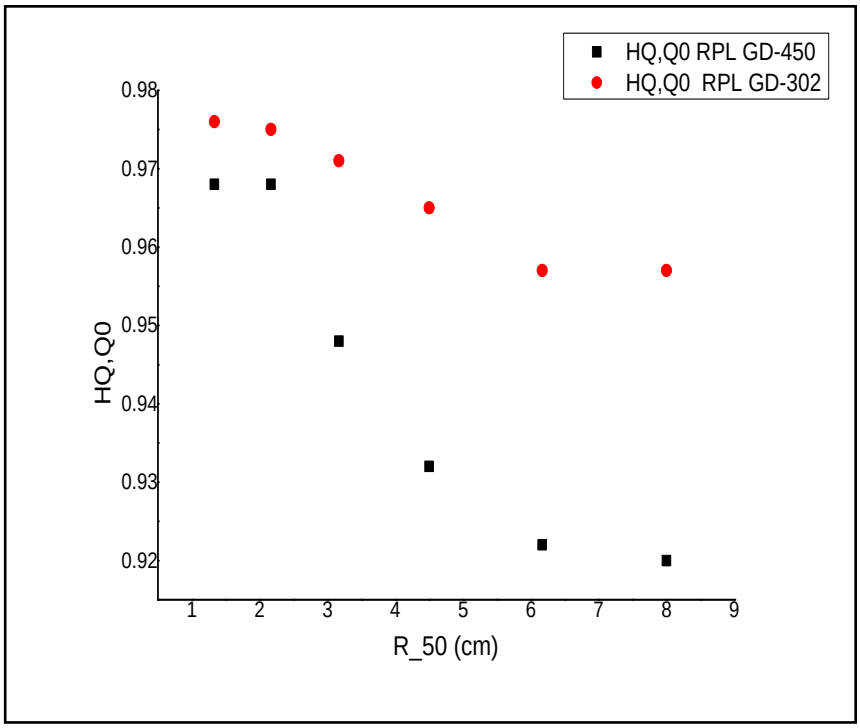

Figure (IV.10): Comparison between of RPL GD-450 with RPL GD-302.

The current study demonstrates that dimension of dosimeter has an important impact on the energy dependence.

For electron beams, Fig.(IV.10) shows the calculated relative responses of both dosimeters in the energy range of 4–20 MeV as a function of beam quality specified, R_{50} (cm). The relative responsesare normalized to the responses per unit dose calculated with a Co-60 beam.

So it can be said, after this results, that the dosimeter Silver-activated phosphate glass without filter can use as a detector with high energy electrons beams such as in radiation therapy.

We recommended that the dosimeters RPLGD-450 and RPLGD-302 must be with energy compensator filters (Aluminum, Copper, Tin…) used for neglected the influence of energy. [6]

GENERAL CONCLUSION

GENERAL CONCLUSION

A radiation dosimeter is a device, instrument or system that measures or evaluates, either directly or indirectly, the quantities exposure, kerma, absorbed dose or equivalent dose, or their time derivatives (rates), or related quantities of ionizing radiation. A dosimeter along with its reader is referred to as a dosimetry system.

To function as a radiation dosimeter, the dosimeter must possess at least one physical property that is a function of the measured dosimetric quantity and that can be used for radiation dosimetry with proper calibration. In order to be useful, radiation dosimeters must exhibit several desirable characteristics.

In radiotherapy exact knowledge of both the absorbed dose to water at a specified point and its spatial distribution are of importance, as well as the possibility of deriving the dose to an organ of interest in the patient. In this context, the desirable dosimeter properties will be characterized by accuracy and precision, linearity, dose or dose rate dependence, energy response, directional dependence and spatial resolution

Due to Monte Carlo method and the amazing results that it showed in radiotherapy domain, has become is the common way in the calculation of absorbed dose (energy deposition). We Have relied on simulation Monte Carlo to calculate the dosimeters responses.

This memory was concerned a passive dosimeter which based on luminescence phenomenon, it's Radiophotoluminescence dosimeters.

We have adopted in current study two Radiophotoluminescence glass dosimeters: RPL GD-450 and RPL GD-302 without filters, both dosimeters are Silver-activated phosphate glass and belong the type FD-7 glass series.

In our work, we were using the Monte Carlo simulation code MCNP5 developed and maintained by Los Alamos National Laboratory (LANL) to calculate the Percentage Depth Dose (PDD%) and energy response in water phantom (dimension of 30x 30x 30 cm3) for 4-20 MeV electrons beams with 60Co γ-ray as a reference beam.

For 4 MeV electrons beam, we found that the depth maximum dose was at depth Z=0.8 cm for RPL GD-302 and water, for RPL GD-450 the depth maximum dose was at depth of 0.9 cm.

For 6 MeV electrons beam, the results show that the maximum depth dose was at depth of 1.4 cm for RPLGD- 450, at depth of 1.5 cm for RPLGD- 302, and at depth of 1.5 cm for water.

The difference between the calculation values in RPL GD-450 and RPL GD-302 is due to the difference of geometry, where its diameters are 8 mm and 1.5 mm, respectively.

Our results confirm that, for constant field size and source surface distance (SSD) the PDD beyond Z_{max} increases with beam energy because of a decrease in beam attenuation.

The Monte Carlo calculations appear an over responses for both RPL GD-450 and RPL GD-302 appeared slow fall, by a maximum of 8 % and 4.3% respectively.

The results show that, energy dependence F_{Q,Q_0} decrease with increase of energy. According to this study, energies responses of 4 - 20 MeV electrons beams were approximately between 2.5% and 4.3% for RPL GD-302 ,and between 3.3% and 8% for RPL GD-450.

The correction factor should be determined for high energy electron beams with RPLGD- 450 and RPLGD- 302 to will be suitable in evaluations, assessments, or for absorbed dose determination such as in radiotherapy.

The current study demonstrates that dimension of dosimeter has an important impact on the energy dependence.

So it can be said, after this results, that the dosimeter Silver-activated phosphate glass without filter can use as a detector with high energy electrons beams such as in radiation therapy.

For neglected the influence of energy, we recommend that the dosimeters RPLGD-450 and RPLGD-302 must be used with energy compensator filters (Aluminum, Copper, Tin…).

As a perspective to this work, we can enlarge the study of the both dosimeters to other dosimetric characteristics parameters such as dose profile, output factor, the percentage depth dose for different field size with different energies…ect, for electrons beams and photons beams.

Supplements

Supplements

1.Cell card

j m d geom params

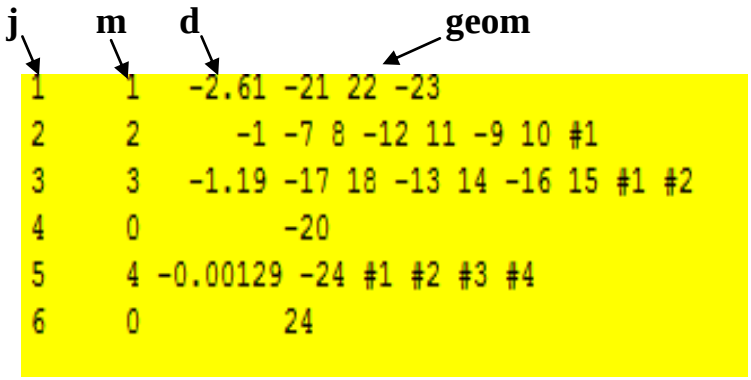

Figure(1): MCNP5 (cell card)

2.Surface card

j a list

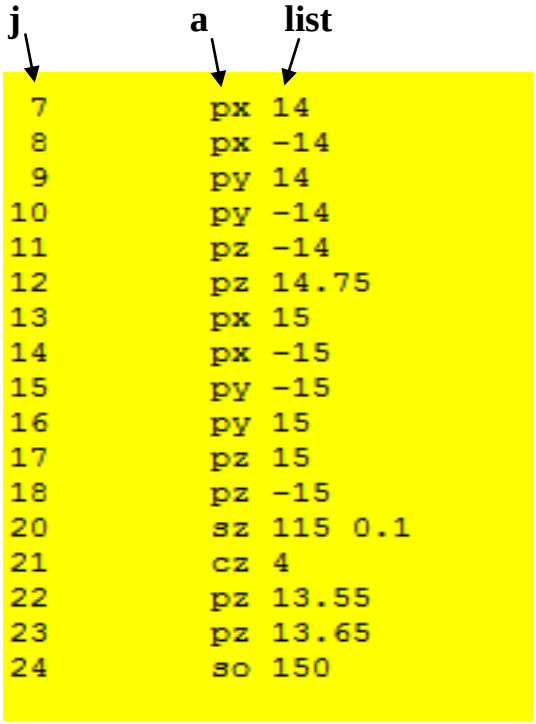

Figure(2): MCNP5 (surface card)

3.Data card

Mn ZAID1 fraction1 ZAID2 fraction2

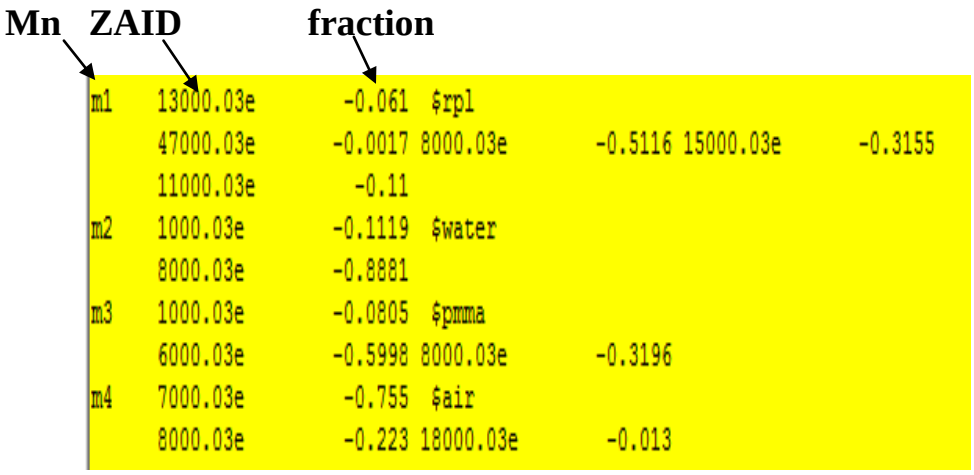

Figure(3): MCNP5 (data card)

4.Source card (sdef)

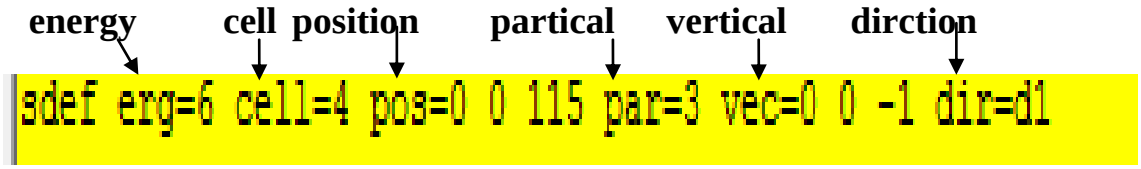

Figure(4): MCNP5 (source card)

5.Problem cutoffs

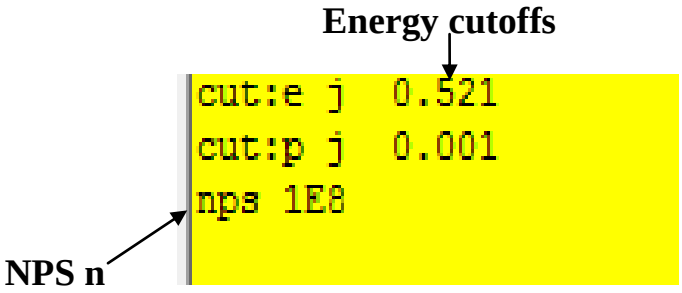

Figure(5): MCNP5 (problem cutoff)

REFERENCES

[1] E.B. Podgorsak "Radiation oncology physics: A handbook for teachers and students", Vienna: Technical Editor, IAEA, (2005).

[2] Y.O. Salem, A. Nourreddine, A. Nachab, C. Roy, A. Pape, "Present state of the art of a fast neutron dosimeter incorporating RPL detectors", Journal of Nuclear Sciences, Ankara University Institute of Nuclear Sciences, Volume 2, No. 2 ISSN: 2148-3981, (2015).

[3]G. Rajan, J. Izewska" Radiation Oncology Physics:A Handbook for Teachers and Students Radiation (Chapter 4 Monitoring Instruments)", IAEA publication.

[4] International Commission on radiation Units and Measurements. Determination of operational dose equivalent for neutrons. ICRU report 66,(2001).

[5] K . Son, H. Jung, S. H. Shin, H.Ho Lee, S. Lee, Mi-Sook Kim, Y. H. Ji, K. B. Kim , "Feasibility Study of the Radiophotoluminescent Glass Dosimeter for High-energy Electron Beams", k NRF, No. 2011-0002305, Korea, (2011).

[6] Faiz M. Khan, "Physics of Radiation Therapy", Third Edition, P.9.67.71-75.297-300.406, 2003.

[7] "Canadian Nuclear Safety Commission (CNSC), Introduction to Radiation", (December 2012).

[8] H. E. Johns, J. R. Conningham, "The physics of radiology",Charles C Thomas, U. S. A, fourth education, (1983).

[9] E.B. Podgorsak, "Radiation Physics for Medical Physicists", Biological and medical physics, biomedical engineering Germany, P.7, (April 2005).

[10] "Principles of Radiation Interactions", https://ocw. mit. edu. 22-55,P.1-4.

[11] C. Levin, "Basic Physics of Radionuclide Imaging, chapter 04", Molecular Imaging Program, Stanford University School of Medicine, Stanford, California, P.65-73.

[12] " AN4 Interaction of radiation with matter", www. Physics. usyd. edu. au, P.51-68.

[13] M, Anna-Leena," Clinical applications of radiophotoluminescence (RPL) dosimetry in evaluation of patient radiation exposure in radiology. Determination of absorbed and effective dose", University of Oulu, Finland, (2014).

[14] Experimental techniques in nuclear and particles physics, ISBN: 978-3-642-00828-3, IX, 306 P., Hardcove, (2010).

[15] H. Hirayama, "Lecture Note on Photon Interactions and Cross Sections", KEK, High Energy Accelerator Research Organization, 1-1, Oho, Tsukuba, Ibaraki, 305-0801 Japan.

[16] F. Krumeich, " Properties of Electrons, their Interactions with Matter and Applications in Electron Microscopy", Laboratory of Inorganic Chemistry, ETH Zurich, Vladimir-Prelog-Weg 1, 8093 Zurich, Switzerland.

[17] J.V. Siebers,"Basic Radiation Interactions, Definition of Dosimetric Quantities, and Data Sources"**,** Virginia Commonwealth UniversityRichmond, Virginia USA,(2009).

[18] " Interaction of Radiation with Matter", Oregan state university online, oreganstate. edu/ Chapter 17.

[19] D.R. Dance et al" Diagnostic Radiology Physics: A Handbook for Teachers and Students Vienna: Technical Editor, IAEA, (2014).

[20] S. M. Seltzer, "Fundamental quantities and units for ionizing radiation (Revised), The international commission on radiation units and measurements", Published by Oxford University Press ICRU REPORT No. 85, Journal of the ICRU Volume 11 No 1,(October 2011).

[21] G. Dietze, K. Eckerman, H. Menzel, J. Stather, C. Streffer, Chairman , "Committee 2: Bbasis for dosimetric quantities used inradiological protection", International Commission on Radiological Protection, (April 2005).

[22] J. Valentin,"The 2007 Recommendations of the International Commission on Radiological Protection", El sevier, (2007).

[23] S. Mattsson , M. Söderberg, "Dose Quantities and Units for Radiation Protection ", Radiation Protection in nuclear Medicine, Matsson, S, Hoeschen, C, (Eds.), VIII, 168 p. , Hardcover ISBN: 978-3-642-31166-6, (2013).

[24] P. Cherry, A. M. Duxbury ,"Practical Radiotherapy", Second Edition, Blackwell Publishing Ltd, 2009.

[25] J. A. Mullens, J. D. Edwards, S. A. Pozzi, " Analyais of scintillator pulse-height for nuclear materials identification", Oak Ridge National Laboratory.

[26] N. Navab Moghadam, S.M. Hosseini Pooya, H. Afarideh, M.R. Kardan, "Response of TLD and RPL personal dosimeters in a national inter-comparison test program", Int. J. Radiat. Res., Vol. 14 No. x, January 2016.

[27] "Ageneral introduction on luminescence", shodhgnga.iffibnet. ac. in/ 08_chapter 1.

[28] L. Nasdala, J. Götze, J. M. Hanchar, M. Gaft & M. R. Krbetschek, " Luminescence techniques in Earth Sciences".

[29] " Thermoluminescence Basics Theory and Applications", www; nucleonix; com/ TldEXP Manual.

[30] "Luminicence: An introduction, www.perkinelmer. co. kr.

[31] Zeljka Knezevic, Liliana Stolarczyk, Igor Bessieres, Jean Marc Bordy. Photon dosimetry methods outside the target volume in radiation therapy: Optically stimulated luminescence (OSL)thermoluminescence (TL) and radiophotoluminescence RPL dosimetry Radiation Measurements 57 pp9-18, (2013).

[32] H. Asni, H. Wagiran, I. Hossain, A. T. Ramli, and M. I. Saripan, "Thermoluminescence Energy Response of TLD-100 Subjected to Photon Irradiation Using Monte Carlo N-Particle Transport Code Version 5", Journal of Engineering Thermophysics, ISSN 1810-2328, Vol. 20, No. 3, pp. 329–333, (2011).

[33] J.-E. Rah , U.-J. Hwang , H. Jeong , S.-Y. Lee , D.-H. Lee , D. H. Shin , M.Yoon , S. B. Lee , R. Lee , S. Y. Park,"Clinical application of glass dosimeter for in vivo dose measurements of total body, Radiation Measurements", irradiation treatment technique, Elsevier, (2011).

[34] J. Seco, B. Clasie, M. Partridge," Review on the characteristics of radiation detectors for dosimetry and imaging", Physics in Medicine & Biology(Phys. Med. Biol), R303–R347, (2014).

[35] S. B. Scarboro, D. S. Followill, J. R. Kerns, R. A. White , S. F. Kry, "Energy response of optically stimulated luminescent dosimeters for non-reference measurement locationsin a 6 MV photon beam", Phys. Med. Biol.57, 2505–2515 , (2012).

[36] "Dose Ace: RPL Glass Dosimeter / Small Element System", International Affairs Section, Chiyoda Technol Corporation, e-mail: kotayashi-t@c-technol.co.jp.

[37] H. Ebendorff-Heidepriem, C.Riziotis , E. Taylor, "Novel photosensitive glasses", Optoelectronics Research Centre, University of Southampton, SO17 1BJ, U.K..

[38] C. Spina, Ph.D, "Silver I, II, III: Chemic al Characteristics , Proper ties , and Antimicrobial Activity", Exciton Technologies Inc. – Edmonton, Alberta, Canada.

[39] David Y.C. Huang, Shih-Ming Hsu, "Radio-Photoluminescence Glass Dosimeter (RPLGD)", InTech, (2011).

[40] I. A. Rahman, M. T. M.i Ayob, H. M. K. Mohd1, A. F Ahmad, S. Sharin, F. Mohamed, S. Ab Aziz, S. Radiman, " Efect of silver nanoparticle addition on the structure and characteristics of radio photoluminescence glass dosimeter", Malaysian Journal of Analytical Sciences, Vol 20 No 1 ISSN 1394 – 2506, 64 – 72, (2016).

[41] E. PIESCH, B. BURGKHARDT, "Photoluminucence dosimetry : the alternative in personnel monitoring", Germany, Radioprotection Vol. 29- 0033-8451, n°l, pages 39 à 37, (1994).

[42] A. AL-BASHEER, "3D deterministic radiation transport for dose computation in clinical procedures", university of Florida, (2008).

[43] "MCNP — A General Monte Carlo N-Particle Transport Code, Version 5 Volume I: Overview and Theory", Diagnostics Applications Group Los Alamos National Laboratory, University of California, (24April 2003).

[44] A. A. Abbott, "Quantum Random Numbers: Cortication and Generation", University of Auckland, (2011).

[45] A. A. Thomas, V. Paul, " Random Number Generation Methods a Survey ", International Journal of Advanced Research in Computer Science and Software Engineering, Volume 6, Issue 1, ISSN: 2277 128X, (January 2016).

[46] M. Vilches , S. Garc´ıa-Pareja , R. Guerrero , M. Anguiano , A.M. Lallena , "Monte Carlo simulation of the electron transport through thin slabs: A comparative study of penelope, geant3, geant4, egsnrc and mcnpx", Spain.

[47] F. Salvat, J. M. Fernández-Varea, J. Sempau, "PENELOPE-2008: A Code System for Monte Carlo Simulation of Electron and Photon Transport", Universitat de Barcelona, Spain, (2008).

[48] Prasada Rao Gurubilli, "Random number generation and its better technique", Master of Engineering, computer science and engineering department, thapar university Patiala – 147004, (June 2010).

[49] "Applied R&M Manual for Defence Systems Part D - Supporting Theory(Chapter 4 Monte-Carlo simulation)", GR-77 Issue, (2012).

[50] J. Sempau , J.M. Fern_andez-Varea , E. Acosta , F. Salvat, "Experimental benchmarks of the Monte Carlo code PENELOPE", Nuclear Instruments and Methods in Physics Research B 207 (2003) 107–123, Elsevier, (2003).

[51] C. A. Adjei, " MCNP5 AND GEANT4 comparisons for preliminary fast neutronpencil beam design at the university of utah triga system", Master of Science, Nuclear Engineering, University of Utah, (December 2012).

[52] W. R. Nelson, H. Hirayama, and D. W. O. Rogers. The EGS4 Code System. Report SLAC,265, Stanford Linear Accelerator Center, Stanford, California, (1985).

[53] A. L. Reed, "Medical physics calculations with mcnp: A primer", Los Alamos National Laboratory, X-3 MCC Texas A&M University, Dept. of Nuclear Engineering Summer American Nuclear Society Meeting Boston, MA, June 25-28, (2007).

[54] J. R. Diago, "Simulation of detector calibration using MCNP", Universidad politécnica de Valencia, ESPAÑA, CHERNE network ,ISIB, Bruxelles (Belgique), (22 November 2005).

[55] J. K. Shultis, "An mcnp primer", R. E. Faw, Dept. of Mechanical and Nuclear Engineering, Kansas State University, Manhattan, KS 66506, (2011).

[56] "MCNP — A General Monte Carlo N-Particle Transport Code, Version 5 Volume II: User's Guide", Diagnostics Applications Group, Los Alamos National Laboratory, University of California, April 24, (2003).

[57] D. B. Pelowitz, "MCNPX$_{TM}$ user's manual", Los Alamos National Laboratory, University of California , Version 2.5.0, (April 2005).

[58] T. Kurobori, Y. Miyamoto, Y. Maruyama, T. Yamamoto, T. Sasaki, "A comparative study of optical and radiative characteristics of X-ray-induced luminescent defects in Ag-doped glass and LiF thin films and their applications in2-D imaging", Nuclear Instruments and Methods in Physics Research B 326 (2014) 76–80, ELSEVIER, (2014).

[59] D.Maki, T. Sakai, Y. Koguchi, H. Ohguchi, W. Sinozaki, N. Juto, "Dependence of the Glass Badge response on the different calibration phantoms", Journal of nuclear science and technology, Supplement 5, p. 183–186 (June 2008).

[60] J.M. Bordy , I. Bessieres , E. d'Agostino , C. Domingo , F. d'Errico , A. di Fulvio , Z. Knezevic, S. Miljanic, P. Olko , A. Ostrowsky , B. Poumarede , S. Sorel , L. Stolarczyk , D. Vermesse, "Radiotherapy out-of-field dosimetry: Experimental and computational results for photons in a water tank",Radiation Measurements, 57 29-34, (2013).

[61] A-H. Benali, G. Medkour, A. Nourreddin, M. Allab, "Comparison of RPL GD-301 and TLD-100 detector responses by Monte Carlo simulation", EPJ Web of conferences 100, 02001, (2015).

[62] P. Andreo, J.P. Seuntjens, E.B. Podgorsak, "Calibration of photon and electron beams", P301-354.

[63] C. V.Chung, T. V.Hung, N. A. Tuan V.X. Cach ,"The Annual Report for 2010: Study on Characteristics of Electron beam on UELR-10-15S2 Accelerator for Commisioning Purpose ", Vietnam Atomic Energy Institute (VAEI), Vietnam.

[64] E.Waldeland , E. Malinen, "Review of the dose-to-water energy dependence of alanine and lithium formate EPR dosimeters and LiF TL-dosimeters-Comparison with Monte Carlo Simulations", Radiation Measurements 46 (2011) 945- 951, Elsevier, (2011).

[65] M. Mahjour, "A New Approach to Cancer Remedy by Radioimmunotherapy with Alpha Particles: A Novel Study", International Journal of Scientific & Engineering Research, Volume 5, Issue 9, September 2014, Pages 788-794.

[66] S. García-Pareja, M. Vilches, A.M. Lallena, "Ant colony method to control variance reduction techniques in the Monte Carlo simulation of clinical electron linear accelerators of use in cancer therapy", Journal of Computational and Applied Mathematics, Volume 233, Issue 6, 15 January 2010, Pages 1534-1541.

[67] S. Chatterjee, A.K. Bakshi, R.A. Kinhikar, G. Chourasiya, R.K. Kher, "Response of CaSO4: Dy phosphor based TLD badge system to high energy electron beams from medical linear accelerator and estimation of whole body dose and skin dose", Radiation Measurements, Volume 44, Issue 3, March 2009, Pages 257-262.

[68] Almond, P. R, "Characteristics of current medical electron accelerator beams", p. 43-53 in Proceedings of the Symposium on Electron Beam Therapy, Chu, F. C. H. and Laughlin, J. S. Eds. (Memorial Sloan Kettering Cancer Center, New York), (1981).

[69] Kirby, T. H., Gastorf, R. J., Hanson, W. F., Berkley, L. W., Gagnon, W. F., Hazle, J. D. and Shalek, R. J, "Electron beam central ax is depth dose measurements", Med. Phys. 12, 357-361, (1985).

[70] J-E. Rah, J-Y. Hong, G-Y. Kimc, Y-L. Kimd, D-O. Shin, T-S. Suh, "A comparison of the dosimetric characteristics of a glass rod dosimeter and a thermoluminescent dosimeter for mailed dosimeter", Radiation Measurements, 44 18–22, (2009).

ملخص:

الغرض من العمل الحالي هو دراسة استجابة اثنين من أجهزة قياس الجرعات الزجاجية (كواشف) المتاحة في السوق و المعروفة باسم RPL GD-302 و RPL GD-450 دون مرشحات.

في هذه الدراسة، قمنا باستخدام برنامج محاكاة مونت كارلو MCNP5 لحساب النسبة المئوية جرعة العمق (PDD%) والاستجابة الطاقوية في مجسم مائي مع حزم الإلكترونات (4-20 MeV) وباستعمال أشعة γ لـ^{60}Co كحزمة مرجعية.

بينت حسابات مونتي كارلو، مع الأشعة ذات الطاقة 4 MeV عمق الجرعة القصوى كان 0.8 سم و 0.9 سم، ومع الأشعة ذات الطاقة 6 MeV كان عمق الجرعة القصوى 1.4 سم و 1.5 سم لـ RPL GD- 450 و RPL GD- 302، على التوالي. من ناحية أخرى، نتائج الإستجابة الطاقوية قابلة للمقارنة مع ما هو منشور في المجلات المحكمة، حيث وجدنا حد أقصى قدره 8٪ و 4.3٪ لـ RPL GD- 450 و RPL GD- 302، على التوالي.

وأخيرا، تؤكد نتائجنا أن جهاز قياس الجرعات الفوسفاتية الفضية المنشطة بدون مرشح يمكن أن تستخدم ككاشف لحزم الإلكترونات عالية الطاقة مثل التي تستعمل في العلاج الإشعاعي.

كلمات بحثية: مقاييس الجرعات راديوفوتولومينزانس، RPL زجاج مقياس الجرعات، محاكاة مونت كارلو، النسبة المئوية جرعة العمق ،الإستجابة الطاقوية، حزم الالكترونات، MCNP5.

Abstract

The purpose of current work was to study the response of two commercially available glass dosimeters known as RPL GD-302 and RPLGD-450 without filters.

In this study, Monte Carlo simulation code MCNP5 was using to calculate the Percentage Depth Dose (PDD%) and energy response in water phantom for 4-20 MeV electrons beams with ^{60}Co γ-ray as a reference beam.

Monte Carlo calculations show, with 4 MeV energy beam the depth of maximum dose was 0.8 cm and 0.9 cm, and with 6 MeV the depth of maximum dose was 1.4 cm and 1.5 cm for RPL GD- 450 and RPL GD- 302 , respectively. In other part, the results energy responses are comparable with literature, where we found a maximum of 8 % and 4.3% for RPL GD- 450 and GD-302, respectively.

Finally, our results confirm that the Silver-activated phosphate glass dosimeter without filter can be used as a detector for high energy electrons beams such as in radiation therapy.

Keywords: Radiophotoluminescence dosimeters, RPL Glass Dosimeter, Monte Carlo simulation, Percentage Depth Dose, PDD, Energy response, Electrons beams, MCNP5.

Résumé

L’objectif du notre travail était d'étudier la réponse de deux dosimètres de verre disponibles dans le marché, connus sous le nom de RPL GD-302 et RPLGD-450 sans filtres.

Dans cette étude, le code de simulation Monte Carlo MCNP5 utilisait pour calculer la pourcentage de dose de profondeur (PDD%) et la réponse énergétique dans un fantôme d'eau pour les faisceaux d'électrons de 4-20 MeV avec rayons γ du ^{60}Co comme faisceau de référence.

Les calculs de Monte Carlo montrent montre, avec un faisceau d'énergie de 4 MeV, la profondeur de la dose maximale était de 0,8 cm et 0,9 cm, et avec 6 MeV, la profondeur de la dose maximale était de 1,4 cm et 1,5 cm pour RPL GD-450 et RPL GD-302, respectivement. D'autre part, les réponses énergétiques des résultats sont comparables à celles de la littérature, où nous avons trouvé un maximum de 8% et 4,3% pour RPL GD-450 et RPL GD-302, respectivement.

Enfin, nos résultats confirment que le dosimètre en verre phosphate activé par l’argent sans filtre peut être utilisé comme détecteur pour des faisceaux d'électrons à haute énergie tels que dans la radiothérapie.

Mots-clés: Dosimètres de radiophotoluminescence, Dosimètre de verre RPL, simulation Monte Carlo, pourcentage de dose de profondeur, PDD, réponse énergétique, faisceau d'électrons, MCNP5.